Conformational Study of (8α,8'β)-Bis(substituted phenyl)-lignano-9,9'-lactones by Means of Combined Computational, Database Mining, NMR, and Chemometric Approaches

5 AUTHORS, INCLUDING:

Rudolf Kiralj
Technical College in Bjelovar
40 PUBLICATIONS   **482** CITATIONS

SEE PROFILE

Paulo Marcos Donate
University of São Paulo
67 PUBLICATIONS   **576** CITATIONS

SEE PROFILE

Rosangela Laurentiz
São Paulo State University
45 PUBLICATIONS   **454** CITATIONS

SEE PROFILE

Sergio Albuquerque
University of São Paulo
126 PUBLICATIONS   **1,843** CITATIONS

SEE PROFILE

Conformational Study of (8α,8′β)-Bis(substituted phenyl)-lignano-9,9′-lactones by Means of Combined Computational, Database Mining, NMR, and Chemometric Approaches

Rudolf Kiralj,[†] **Márcia M. C. Ferreira,*,**[†] **Paulo M. Donate,**[‡] **Rosangela da Silva,**[§] **and Sergio Albuquerque**[§]

Instituto de Química, Universidade Estadual de Campinas, 13083-970 Campinas, SP, Brazil, Departamento de Química da Faculdade de Filosofia, Ciências e Letras de Ribeirão Preto, Universidade de São Paulo, 14040-901 Ribeirão Preto, SP, Brazil, and Faculdade de Ciências Farmacêuticas de Ribeirão Preto, Universidade de São Paulo, 14040-903 Ribeirão Preto, SP, Brazil

Received: October 13, 2006; In Final Form: April 10, 2007

β-(3,4-Methylenedioxybenzyl)-γ-butyrolactone (MDBL) and (−)-hinokinin (HK) were obtained by partial synthesis and characterized by ^{1}H NMR and computational methods (conformational analysis, molecular modeling, structural data mining and chemometrics). Three conformers were detected for MDBL and nine were found for HK. The energy differences are around 1 and 2 kcal mol^{-1} and rotation barriers are less than 3 and 5 kcal mol^{-1} for MDBL and HK conformers, respectively. The geometries of these conformers, obtained from semiempirical PM3 and density functional theory (DFT) B3LYP 6-31G** calculations agree satisfactorily with ^{1}H NMR data (vicinal proton−proton coupling constants) and structures retrieved from the Cambridge Structural Database (torsion angles). DFT combined with some variants of the Haasnoot−de Leeuuw−Altona equations gives the best predictions for the coupling constants. The molecular conformation of MDBL, of HK, and of related systems depends not only on intramolecular interactions but also on crystal packing forces and solvent−solute interactions, in particular hydrogen bonds and polar interactions. Hydration favors more stable HK conformers, which can be important for their behavior in chemical and biological systems.

1. Introduction

Lignans have attracted much interest over the years and are still being intensively investigated because of their wide occurrence in nature (mainly in the plant kingdom), and also because of their broad range of biological activities with therapeutic potential.[1−5] Lignans exibit effects on various organisms including humans at molecular, enzymatic, physiological, pharmaceutical, and even clinical level.[1−8]

The (8α,8′β)-bis(substituted phenyl)lignano-9,9′-lactones[9] are a subclass of dibenzylbutyrolactone lignans with a series of interesting conformational features, such as the existence of various flexible bonds and the possibility of hydrogen bonding and interaction between substituted aromatic C$_6$ units (phenyl rings). The C$_6$ units might, to a certain extent, sterically hinder each other or exhibit other types of interaction with the γ-butyrolactone ring. In this way, conformational analysis for these compounds could provide information about such interactions and their influence on the preferential conformations.

Conformational studies of (8α,8′β)-lignano-9,9′-lactones, particularly of their precursor (8′β)-(3′,4′-methylenedioxybenzyl)-γ-butyrolactone (MDBL, Figure 1) and of (8α,8′β)-3,4,3′,4′-bis(methylenedioxy)lignano-9,9′-lactone or (−)-hinokinin (HK, Figure 2), have been performed in this work to give a new insight into lignan lactone conformational flexibility and conformer distribution. Among most frequent approaches to
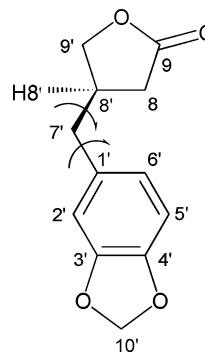

Figure 1. Molecular structure of (8′β)-(3′,4′-methylenedioxybenzyl)-γ-butyrolactone (MDBL) with atomic numbering and definition of the studied rotation angles.
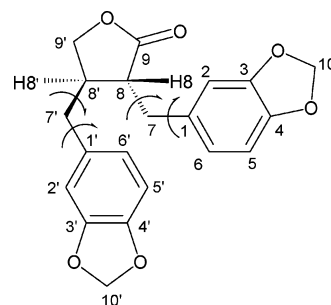
Figure 2. Molecular structure of (−)-hinokinin (HK) with atomic numbering and definition of the studied rotation angles.

conformational analysis known in literature, are structural approaches employing structural databases[10−14] and sometimes chemometric methods,[15] coupled structural-computational,[16] and computational−NMR approaches.[17−20] Data mining using the

* Corresponding author. Telephone: +55 19 3521 3102. Fax: +55 19 3521 3023. E-mail: marcia@iqm.unicamp.br.
† Instituto de Química, Universidade Estadual de Campinas.
‡ Departamento de Química da Faculdade de Filosofia, Ciências e Letras de Ribeirão Preto, Universidade de São Paulo.
§ Faculdade de Ciências Farmacêuticas de Ribeirão Preto, Universidade de São Paulo.

Conformational Study of Lignanolactones

J. Phys. Chem. A, Vol. 111, No. 28, 2007 **6317**

Cambridge Structural Database (CSD)[10,14,17,21,22] for compounds structurally related to MDBL and HK, was performed in this work. Although crystal packing effects on internal coordinates, molecular conformation and other structural properties are noticeable in general,[13,23−26] molecular geometries retrieved from the CSD are usually a good guide to conformational preference in aqueous solution or at protein binding sites.[10−12] Furthermore, various molecular modeling packages employ molecular structures or structural data from the CSD.[27−32] Conformational analysis for MDBL and HK was carried out at a semiempirical (method with PM3 Hamiltonian[33]) and density functional theory (DFT[34] method with the B3LYP[35,36] functional) levels in vacuum. Both compounds have been synthesized, their NMR spectra were recorded and then coupled to computational procedures in order to determine the conformational composition of these compounds in solution.

2. Computational Methods

Systematic Conformational Analysis for (8′β)-(3′,4′-Methylenedioxybenzyl)-γ-butyrolactone (MDBL). (8′β)-(3′,4′-Methylenedioxybenzyl)-γ-butyrolactone (MDBL, Figure 1) is a typical representative of lignan lactone precursors with a lignan C_6 unit (methylenedioxybenzyl) on the γ-butyrolactone ring at position 8′. The IUPAC atom numbering for MDBL was adapted to be consistent with the lignano-9,9′-lactone numeration system for comparative purposes. The exocyclic methylene group (C7′) in lignano-9,9′-lactones is characterized in literature and also in this work by two $^3J_{HH}$ coupling constants from ^1H NMR spectra, accounting for interactions between H8′ and the methylene protons H7′a and H7′b. The conformers differ mainly in the relative position of the methylenedioxybenzyl groups with respect to the γ-butyrolactone ring (two rotatable single bonds C1′−C7′ and C7′−C8′) which undergoes limited conformational changes. Hence, it can be assumed that ^1H NMR measurements may provide useful information about the conformational composition of these compounds in solution. The presence of methyl, methoxy or other small flexible groups attached to the aromatic C_6 unit in MDBL derivatives increases the number of possible rotations. However, such new groups would not alter the main trends in molecular energy-rotation angle curves relative to those for MDBL. Therefore, conformational analysis of MDBL can be useful for interpreting the conformational behavior of general lignano-9,9′-lactones.

A semiempirical study with PM3 Hamiltonian on MDBL was performed as a fast procedure that enables detection of conformers location on the potential energy curve or surface. The conformational space was scanned by rotating the C_6 unit around the C7′−C8′ and C1′−C7′ bonds. The initial MDBL structure was modeled by using Titan,[37] the rotation angle C1′−C7′−C8′−H8′ was varied from 0 to 350° by 10° increments, and each optimized geometry was obtained with the torsion angle constrained.

The heat of formation was calculated for each conformation with optimized geometry. Additionally, narrow regions around the extremes (conformers and energy barrier peaks) were refined, and new conformations with angle increments of 5° or 2.5° were treated as described above. The most stable conformers were then identified from the heat of formation vs rotation angle plot. Furthermore, the conformer geometries were refined (dihedral constraints excluded).

Molecular visualization and visual inspection of molecular features in this work were performed by using Titan, WebLab ViewerPro 4.0,[38] and Chem3D Ultra 6.0[39] packages.

In order to investigate the possible positions of the methylenedioxybenzyl group with respect to the methylene group, an additional analysis was performed by studying the dependence of the heat of formation on the rotation angle C6′−C1′−C7′−C8′ (Figure 1) for the most stable conformer obtained so far.

Systematic Conformational Analysis for (—)-Hinokinin (HK). (−)-Hinokinin (HK) or (8α,8′β)-3,4,3′,4′-bis(methylenedioxy)lignano-9,9′-lactone is an analogue of MDBL, with two chemically identical lignan C_6 units at positions 8 and 8′ (Figure 2). HK is a simple representative of lignano-9,9′-lactones derived from MDBL-like precursors, and thus is suitable for systematic conformational analysis.

A PM3 semiempirical study was performed on HK in an analogous way as for MDBL by using Titan, changing the rotation angles Θ_1 (C1′−C7′−C8′−H8′) and Θ_2 (C1−C7−C8−H8) from 0° to 350° by 10° increments. In this way, 1296 optimizations (36 × 36) were performed. The obtained surface energy × Θ_1 × Θ_2 was analyzed by Pirouette[40] and Matlab[41] to identify minima, rotation barriers and saddle points. The minima were further geometry-optimized at the PM3 level with the constraints in Θ_1 and Θ_2 removed.

Two additional conformation analyses were performed by studying the change in the heat of formation with rotation angles C6′−C1′−C7′−C8′ and C6−C1−C7−C8 (Figure 2) for the most stable conformer obtained from the above conformation study.

Cambridge Structural Database Mining for MDBL- and HK-Related Structures. In general, crystal structures of small molecules might aid in understanding which conformations of HK and other analogue lignano-9,9′-lactones are predominant in the liquid phase or in complexes with biomacromolecules.[10−12] For this purpose, two systematic searches were performed in the Cambridge Structural Database (CSD)[10,14,17,21,22] January 2006 update:[42] one for substituted 8′,8-bisbenzyl derivatives of γ-butyrolactone and tetrahydrofuran lignans as well as other MDBL-related compound, and another for lignano lactones and other HK-related substances. The data mining was carried out using program ConQuest 1.7[43,44] for fragment search, under conditions as defined in Scheme A in Supporting Information. Raw data sets were then filtered manually, according to adopted structural criteria to create homogeneous and chemically informative data sets. The torsion angles (Scheme A), analogues of rotational angles defined in Figure 1 and 2, were measured by ConQuest in a repeated search, and also by Titan for those structures that did not have hydrogen at required positions and thus had to be modeled first. Crystal symmetry and other crystallographic items (position in the unit cell, asymmetric unit, disorder, redeterminations) were taken into account to create as much as possible large data sets of torsion angles. Fast molecular visualizations inside the CSD system were made by Mercury,[43,45] and the torsion angle statistics by Vista.[46] Selected structures were optimized at the semiempirical PM3 level in order to evaluate the crystal packing effects on molecular conformation. More rigorous evaluation of the crystal packing effects was performed in two analyses. In the first analysis, a MDBL-like compound was selected. A single molecule and molecular aggregates from its crystal structure were treated at various computational levels available in the Titan and Chem3D.[39] In the second analysis, the deviations of the PM3 rotational angles from experimental values (ΔΘ) for all selected MDBL- and HK-like compounds were studied as functions of molecular geometry and crystal packing parameters calculated by using PLATON.[47,48] Related statistical analyses[49−51] for MDBL were performed using Pirouette.[40]

Basis Set Selection and Calculation of $^3J_{HH}$ Coupling Constants for Methylene—Butyrolactone Interactions. A basis set convergence study at the B3LYP level was performed

TABLE 1: Basis Set Convergence at the B3LYP Level of the Molecular Geometry of MDBL[a,b]

basis set	rms(D)/Å[c]	rms(A)/deg[c]	rms(T)/deg[c]	Θ/deg[d]	$\Phi_{CP\gamma}$/deg[e]	Δk_γ[f]	ΔC8/Å[g]	Φ_{CPO}/deg[e]	Δk_O[f]	ΔC10′/Å[g]	E_{SCF}/au[h]
STO-3G	0.053 (10.6)	1.9 (6.3)	2.6 (8.7)	59.0	65.6	0.18	−0.441 (13.7)	planar	planar	+0.011 (19.3)	−755.600789
3-21G*	0.031 (6.2)	1.6 (5.3)	2.6 (8.7)	62.5	246.9	0.14	+0.557 (25.0)	planar	planar	−0.018 (18.2)	−761.177561
6-31G*	0.018 (3.6)	1.5 (5.0)	0.7 (2.3)	59.4	248.7	0.09	+0.488 (2.0)	323.8	0.01	−0.189 (10.3)	−765.384684
6-31G**	0.018 (3.4)	1.4 (4.7)	0.8 (2.7)	59.5	248.4	0.10	+0.489 (2.3)	324.0	0.00	−0.197 (11.7)	−765.401658
6-31+G*	0.017 (3.4)	1.1 (3.7)	0.5 (1.7)	60.4	70.1	0.05	+0.486 (1.3)	288.0	0.00	−0.289 (27.0)	−765.411946
6-31+G**	0.017 (3.4)	1.0 (3.3)	1.2 (4.0)	60.0	67.7	0.12	+0.473 (3.0)	323.7	0.01	−0.286 (26.5)	−765.428235
6-311G*	0.016 (3.2)	1.4 (4.7)	2.0 (6.7)	62.0	246.1	0.16	+0.466 (5.3)	323.6	0.01	−0.277 (25.0)	−765.563460
6-311G**	0.016 (3.2)	1.4 (4.7)	0.9 (3.0)	62.7	247.1	0.12	+0.485 (1.0)	323.2	0.02	−0.282 (25.8)	−765.580328
6-311+G*	0.015 (3.0)	1.4 (4.7)	0.5 (1.7)	63.0	249.5	0.07	+0.495 (4.3)	322.9	0.03	−0.296 (28.2)	−765.579102
6-311+G**	0.016 (3.2)	1.4 (4.7)	1.0 (3.3)	59.0	249.0	0.08	+0.507 (7.7)	324.3	0.01	−0.281 (25.7)	−765.595872
PM3	0.018 (3.6)	2.4 (8.0)	19.3 (64.3)	52.5	planar	planar	+0.012 (156.7)	planar	planar	+0.002 (47.8)	
experimental[i]				52.0			±0.482 (3)			±0.127(6)	

[a] For more details about the presented parameters and the experimental structures see Table A in Supporting Information. [b] Number in brackets: experimental estimated standard deviations (esd) in the last line. In other lines, the numbers in brackets are ratios of experimental-calculated deviations and the experimental esd, indicating good computation when the ratio is below 3.0. [c] Root-mean square deviations of computed from experimental bond lengths (rms(D)), bond angles (rms(A)) and selected torsion angles (rms(T)). [d] Rotation angle H8′−C8′−C7′−C1′. [e] The Cremer-Pople puckering parameter Φ[55] for five-membered rings: for the γ-butyrolactone ring ($\Phi_{CP\gamma}$) and for the methylenedioxy ring (Φ_{CPO}). [f] Difference between the closest integer and actual value of k defined by $\Phi = k\,360°$ for the γ-butyrolactone (Δk_γ) and the methylenedioxy (Δk_O) rings. [g] Deviation of the envelope's carbon atom from the least-squares plane of other four atoms in the five-membered rings. The numeration is according to that in Figure 1. Positive deviation means that the envelope is turned "up" and the negative deviation that the envelope is oriented "down" from the plane that coincides with the plane of the paper and orientation as in Figure 1. [h] Electronic energy in atomic units (Hartrees). [i] Experimental values to which computed results should approach.

for the molecular geometry of MDBL in order to select the most suitable B3LYP procedure for refining geometries and calculating energies for MDBL and HK conformers. In the first stage of this study, experimental geometry parameters for MDBL were provided. Since there is no crystal structure of MDBL, searches for the most relevant and similar structures were performed in the CSD using ConQuest[43,44] and Vista programs.[46] It is known from structural chemistry[13] that the least affected structural parameters by crystal packing effects are bond lengths, followed by bond angles and torsion angles in rigid substructures (rings, aromatic planes, constrained systems etc.), and finally the most affected are torsion angles connecting such substructures or those having sterically unhindered rotation. In the case of MDBL, HK and analogous compounds, significant crystal packing effects one can expect on torsion angles around the bonds C1−C7, C1′−C7′, C7−C8, and C7′−C8′. Therefore, suitable crystal structures can serve as the experimental reference for MDBL. In the first series of searches (Scheme B in the Supporting Information), the envelope conformations of the two five-membered rings in MDBL, were studied: the distance of atom C8 from the other four atoms of the γ-butyrolactone ring was detected as a local maximum around 0.55 Å (Figure A left, Supporting Information). The most frequent analogous distance for C10′ in the methylenedioxy ring was close to zero, while the frequency decreased continuously with the deviation values (Figure A right). The second series of CSD searches resulted in three crystal structures (CSD REFCODES: DEHQIQ,[52] GEBJOM,[53] and VOQROI[54]) determined in similar conditions, with essential fragments of MDBL that could be used together as the unique experimental reference (Figure B and Table A in the Supporting Information). Essential internal coordinates including bond lengths and bond angles, torsion angles, envelope deviations as well as Cremer−Pople puckering parameters[55] for the five-membered rings were obtained from B3LYP calculations (Table B) and compared with the experimental and PM3-based values in Table 1. The basis set 6-31G** provides acceptable conformation parameters, especially the envelope deviations which are overestimated by the higher basis sets, and at the same time these basis sets do not bring significant improvement in other internal coordinates. According to previous studies for detection of the most suitable basis set by means of chemometric methods,[24,56,57] a data set was built from the
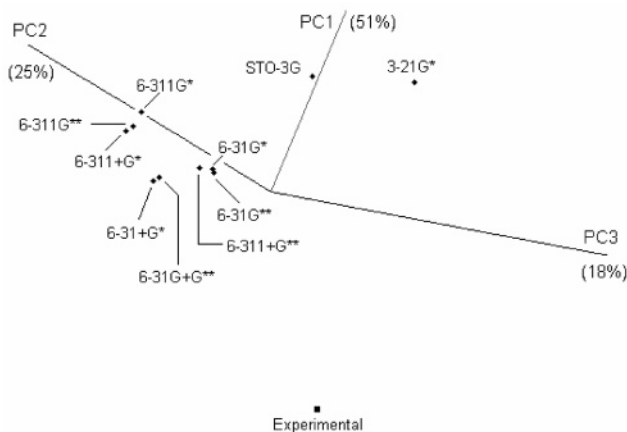

Figure 3. PC1−PC2−PC3 scores plot used for final selection of the B3LYP basis set for further calculations. This PCA was based on rms, Δ, and Θ parameters in Table 1, using absolute values and zero values for experimental rms.

data in Table 1: absolute values of rms and Δ parameters and the rotation angle Θ for all B3LYP basis sets and experiment (rms errors set to zero). The matrix (11 × 6) was treated by means of principal component analysis (PCA).[49−51] The scores space (Figure 3) shows that five basis sets are the closest to the experiment, among which 6-31G** seems to present the best compromise between simplicity, quality, and computational time, and at the same time describes satisfactorily well hydrogen atoms that are important for the study. Therefore, this basis set was selected for all further work.

The conformer distributions at room temperature for *m* conformers obtained from PM3 or from B3LYP computations were determined using the following expressions:

$$w_1 + w_2 + \cdots + w_m = 1$$
$$w_1 = N_1/N, \; w_2 = N_2/N, \; \cdots, \; w_m = N_m/N$$

$$N_i = N_{min} \exp[-(E_{min} - E_i)/kT], \quad N = N_1 + N_2 + \cdots + N_m$$

Here w_i is the molar fraction of the *i*th conformer among *m* conformers; N_i is the population of the *i*th conformer among *m* conformers, *N* is the population of all *m* conformers, N_{min} is

Conformational Study of Lignanolactones

J. Phys. Chem. A, Vol. 111, No. 28, 2007 **6319**

SCHEME 1: Reagents and Conditions in Synthesis of MDBL and HK[a]
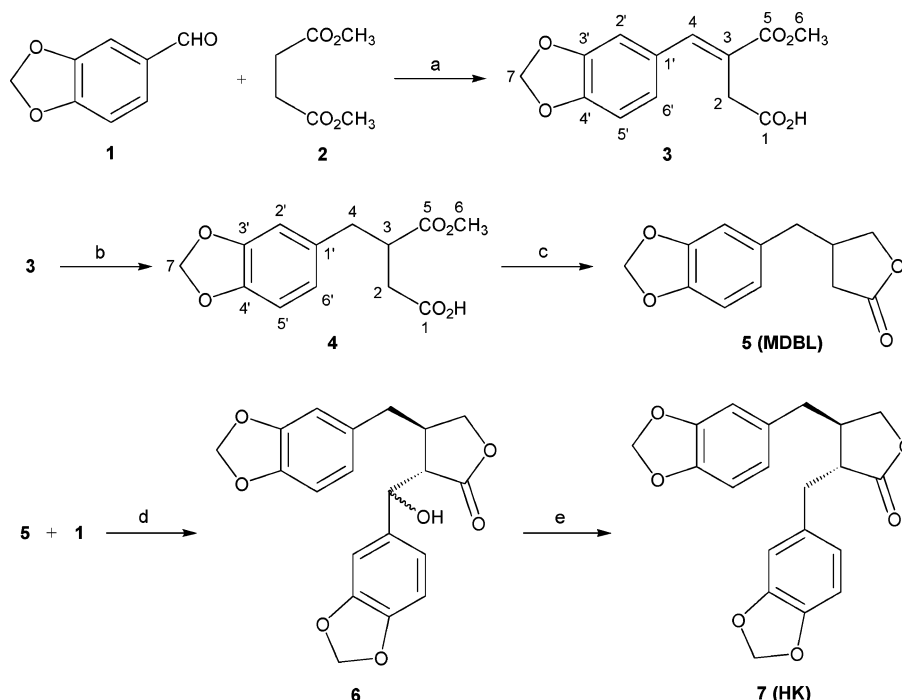
[a] Key: (a) CH_3OH, CH_3ONa, reflux, 5 h, 75%; (b) H_2 (20 atm), 5% Pd/C, CH_3OH, room temperature, 24 h, 90%; (c) (i) KOH, C_2H_5OH, (ii) $Ca(BH_4)_2$, C_2H_5OH, room temperature, h, (iii) HCl, 15 min, 89%; (d) LDA (2 equiv), THF, −78 °C, 4 h, 85%; (e) H_2 (4 atm), 5% Pd/C, CH_3OH, $HClO_4$, room temperature, 60 h, 80%.

the population of the global minimum energy conformer, E_i and E_{min} are the heats of formation or electronic energies of the *i*th and minimum energy conformers, respectively, T is the room temperature in kelvin, and k is the Boltzmann constant.

The vicinal $^3J_{HH}$ coupling constants accounting for methylene−butyrolactone interactions in MDBL and HK were determined experimentally in this study and also taken from the literature. In order to compare the results from the conformational analysis for MDBL and HK with experimental $^3J_{HH}$ constants, an online software program[58] based on the equation published by Haasnoot et al.[59,60] and the MestReJ program,[20] including 11 other equations, were used for calculation of the coupling constants for H7′a/H7′b−H8′ and H7a/H7b−H8 interactions in each conformer. The final average values (weighted by conformer molar fractions) for all equations were compared with available experimental values.

PCA[49−51] was applied to the data matrix consisting of calculated and experimental coupling constants $^3J_{HH}$ for two and four methylene protons from MDBL and HK, respectively. These analyses[24,56] were performed on autoscalled data matrix in order to visualize which computational method provides the closest results to experimentally determined values and also to resolve the ambiguity which proton should be designated "a" and "b". Pirouette[40] was used in all chemometric analyses.

3. Results and Discussion

Chemistry. Several routes for the synthesis of dibenzylbutyrolactone lignans have been reported. In this work, a monosubstituted butyrolactone was synthesized by using the procedure described by Landais et al.[61] The 3′,4′-methylenedioxybenzyl-γ-butyrolactone (MDBL, **5**) was prepared in three steps from the commercially available piperonal (**1**), as outlined in Scheme 1. Stobbe condensation between **1** and dimethylsuccinate (**2**) afforded the unsaturated hemiester **3** in 75% yield which was subsequently hydrogenated over 5% palladium on activated

carbon powder to give the corresponding saturated hemiester **4** in 90% yield. Chemoselective reduction of the potassium salt of **4** with calcium borohydride in ethanol followed by acidic treatment gave the desired lactone **5** in 89% yield (60% overall yield calculated from piperonal). Hinokinin (**7**) was prepared from MDBL (**5**) in 68% overall yield by a two-step procedure involving first the condensation of **5** with piperonal (**1**) in the presence of LDA, producing a mixture of epimeric alcohols **6** in 85% yield, followed by hydrogenolysis to remove the hydroxyl group of **6** to provide hinokinin in 80% yield (Scheme 1).

Computational and Structural Conformational Analysis for (8′β)-(3′,4′-Methylenedioxybenzyl)-γ-butyrolactone (MDBL). Three conformers **I**−**III** of MDBL (Figure 4), representing three conformer types −*gauche* (−*g*), *trans* (*t*) and +*gauche* (+*g*), respectively (Figure 5), were detected when the rotation angle C1′−C7′−C8′−H8′ (Figure 1) was varied. Conformational characterization of the conformers **I**−**III** is presented in Table 2. **I** and **III**, practically of the same energy (differences within 0.2 kcal mol^{-1} in all methods), have the methylenedioxyphenyl unit (substituent R in Figure 5) in −*g* and +*g* position relative to the H8′−C8′ bond, respectively. Consequently, R in these conformers is in *t* and ±*g* positions with respect to the two C8′−C8 and C8′−C9′ bonds of the γ-butyrolactone ring. **II** has R in *t* position with respect to H8′, but in ±*g* with respect to the neighboring C−C bonds of the γ-butyrolactone ring. **II** is characterized by H···H steric interactions between the γ-butyrolactone ring and C_6 unit at rather short distances (Figure 5, Table 2). These interactions are visible in Figure 4 as a shoulder close to **II** as obtained when using the PM3 method. This method, due to its limited basis set, does not treat adequately intermolecular interactions within the γ-butyrolactone ring and methylenedioxy rings which stay planar in all conformers. However, using the B3LYP 6-31G** method, both rings adopt envelope conformations that
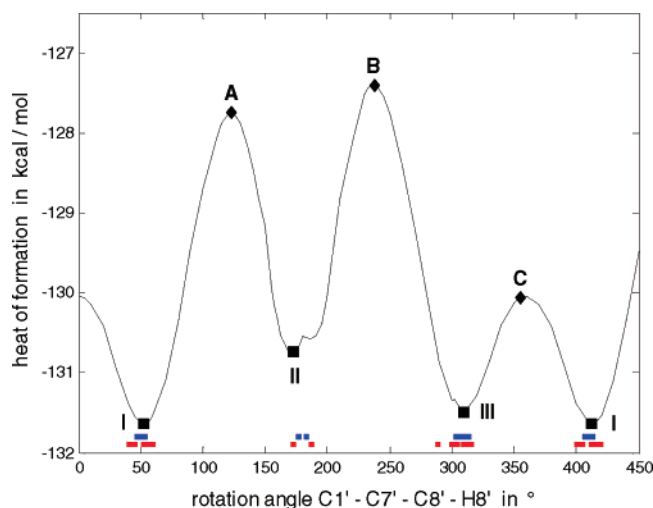
Figure 4. Heat of formation - rotation angle C1′−C7′−C8′−H8′ plot for MDBL from PM3 calculations. Three conformers (**I**, **II**, and **III**) and four rotation barriers (**A**, **B**, **C**, and **D**) are visible. The original plot was extended from 360° to 450° that the relationship between **I** and **III** would be more visible. Selected crystal structure data from the CSD are placed at the bottom of the plot (red squares) together with their PM3-optimized analogues (blue squares).
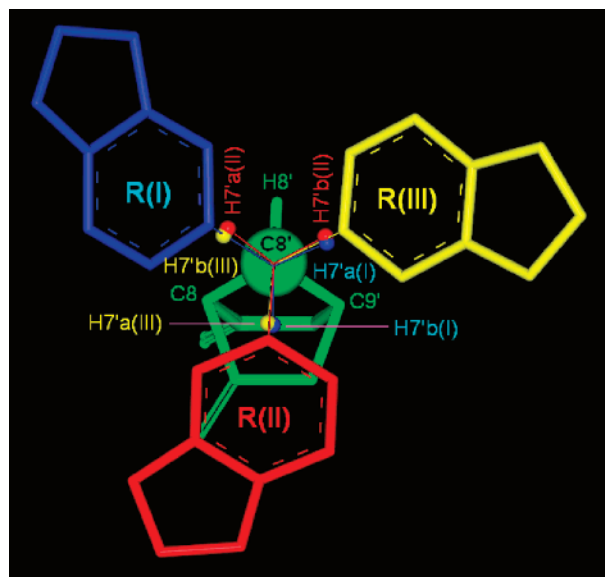

Figure 5. Newmann projection along the C7′−C8′ bond in conformers **I**−**III** of MDBL as obtained from DFT calculations. The substituent R is the methylenedioxyphenyl group colored differently for the three conformers: blue for **I**, red for **II**, and yellow for **III**.

correspond to experimental data (Table 2, Tables A and B in the Supporting Information). The γ-butyrolactone ring is in conformation of "down" envelope at C8′ in **II** to minimize steric repulsions between the two rings (Figure 5). However, this conformation is slightly changed in **I** while it inverts into "up" in **III** (Table 2). The small energy difference between **I** and **III** (Table 2) is probably a consequence of approximate mirror symmetry relationship between the conformers and small influence of the C=O group on the ring inversion. However, it stays unclear why the envelope inverts in **I** ↔ **III** transition.

Rotation barriers around the conformer **II** are **A** (PM3, 2.81; DFT, 3.40 kcal mol⁻¹) and **B** (PM3, 3.14; DFT, 3.76 kcal mol⁻¹). Transitions of **I** and **III** into **II** require 3.87/4.01 and 4.06/4.45 kcal mol⁻¹, respectively, as obtained from PM3/DFT calculations. The energies for transitions **I** ↔ **III** are lower, being 1.42/3.32 and 1.56/3.24 kcal mol⁻¹ as obtained from PM3/DFT

calculations. These results fairly agree with those from parent and related systems. "Up"−"down" envelope inversion of γ-butyrolactone has been reported with barrier of 1.9[62,63] and 2.2[63] kcal mol⁻¹, above which are the **I** ↔ **III** barriers from DFT calculations. Barriers for internal rotation of the methyl group in 8′-methyl-γ-butyrolactone and 8-methyl-γ-butyrolactone have been reported to be 4.1[65] and 3.5[66] kcal mol⁻¹, respectively, which is comparable with the **A** and **B** barriers for MDBL.

It is apparant from Table 2 that the conformational composition **I**:**II**:**III** favored by PM3 is 5:1:4, but the more exact DFT method with the zero-point and thermal corrections yields the opposite composition, 4:1:5. All conformers exist at room temperature in substantial proportions and therefore have to be taken into account for calculation of vicinal ³J_{HH} coupling constants.

The data mining in the Cambridge Structural Database, according to the criteria in Scheme A from the Supporting Information, resulted in a rather large data set of torsion angles for MDBL-related structures (737 angle data). However, torsion angles from the structures most similar to MDBL make a small set (see Figure C in the Supporting Information and Table 3, with torsion angles expressed in the range of 0−360° as rotational angles in Figures 1 and 2). In these structures, three general Q atoms in the central 5-membered ring are carbon atoms (see Scheme A for fragment definition), while the fifth Q atom, the analogue of the epoxy O in MDBL, is the only that varies. Nine from ten structures have the C₆ unit at position 8 and not at 8′ (structure VOQROI). When the torsion angles for these structures, both experimental and PM3 computed data, are superimposed with the energy profile curve (Figure 4), a clear tendency of data grouping at minima can be observed. PM3 data are relatively better grouped than experimental data due to the inexistence of crystal packing effects. It is obvious that both data sets indicate that the conformers +g, t, or −g are the only possible in terms of R relative to the central ring.

When the statistics of the complete data set is presented in the form of a histogram (Figure 6), the correlation between the conformational analysis for MDBL in Figure 4 and conformational behavior of MDBL-like structures in the solid state, is well noticeable. It seems that +g and −g conformers from the CSD have approximately the same total frequency (the area of the corresponding histograms), while the t conformers occur rarely. Furthermore, there are no structures in the range between −g and t or +g and t, but they exist in the range between −g and +g. This is due to the structures with sp² carbon spacer between the C₆ and central rings or with flat substituents at the adjacent positions 8 and/or 9′. These facts are in accordance with the results from computational conformational analysis where **I** and **III** have practically the same energy and **II** is less stable, while the energy barriers for transitions **I** ↔ **II** and **II** ↔ **III** are greater than the barrier for transition **I** ↔ **III**. It is apparant (Table 3) that the differences between torsion angle values in crystal and vacuum (from PM3 calculations) are minor, ranging from 0 to 14°, and therefore, the crystal packing effect and differences among computational and experimental methods do not override the observed conformational trends of MDBL-like systems. The large data set (Figure 6) enables further generalization of these observations. Three conformer types (+g, t, and −g) are the most frequent or even exclusive conformers in systems in which a general ring, not necessarily a carbon ring and not always flat, is separated by sp³ or sp² carbon from the five-membered ring that also may contain various nonmetal atoms besides carbon (see Scheme A in the Supporting Information).

Conformational Study of Lignanolactones

J. Phys. Chem. A, Vol. 111, No. 28, 2007 **6321**

TABLE 2: Computational Conformational Summary for Conformers I-III of MDBL

properties	I	II	III
molecular conformation[a]	$-g$	t	$+g$
Θ (H8′−C8′−C7′−C1′)[b]	52.52°/59.47°	171.32°/178.07°	310.00°/299.34°
lactone conformation[c]	"up" C8′-envelope	"down" C8′-envelope	"down" C8′-envelope
ΔC8′/Å[d]	+0.473	−0.507	−0.490
d(CH$_2$···H$_2$C)/Å[e]	≥ 2.468	≥ 2.935	≥ 2.500
d(ArH···H$_2$C)/Å[f]	≥ 2.632	≥ 2.578	≥ 2.770
E_{PM3}/kcal mol^{-1} [g]	−131.632	−130.744	−131.486
E_{DFT}/kcal mol^{-1} [h]	0.072	0.684	0
E_{DFTZ}/kcal mol^{-1} [h]	0.116	0.855	0
E_{DFTZT}/kcal mol^{-1} [h]	0.105	0.956	0
w_{PM3}[i]	49.88%	11.14%	38.98%
w_{DFT}[j]	40.23%	14.33%	45.44%
w_{DFTZ}[j]	39.94%	11.48%	48.59%
w_{DFTZT}[j]	41.12%	9.78%	49.10%

[a] Molecular conformation is defined by the position of the 3,4-methylenedioxybenzyl group relative to the γ-butyrolactone ring, expressed at the rotation angle Θ or H8′−C8′−C7′−C1′. [b] The angle Θ values that were obtained from PM3/DFT (B3LYP 631G**) geometry optimization. [c] Conformation of the γ-butyrolactone ring is expressed as the envelope at C8′ which is turned "up" or "down" from the plane of the other four ring atoms, as obtained from the DFT calculations. These conformations are known in the literature under the names "bent axial" and "bent equatorial", respectively. The plane coincides with the plane of the paper when molecular formula of MDBL (Figure 1) is viewed. [d] Deviation of atom C8′ from the least-squares plane of the other four atoms of the γ-butyrolactone ring, as obtained from the DFT calculations. [e] H···H distances between the C7′ methylene group and methylenes of the γ-butyrolactone ring, calculated for the DFT-based geometry. [f] H···H distances between the benzene ring and methylenes of the γ-butyrolactone ring, calculated for the DFT-based geometry. [g] Heat of formation from the PM3 geometry optimization. [h] Electronic energies relative to the most stable conformer, calculated from the DFT (B3LYP 6-31G**) geometry optimization: uncorrected electronic energy (E_{DFT}), electronic energy corrected for the zero-point energy (E_{DFTZ}) and electronic energy corrected both for the zero-point energy and thermal energies (translational, rotational and vibrational at 298.15 K). [i] Conformational composition calculated from PM3-based heats of formation. [j] w_{DFT}, w_{DFTZ}, and w_{DFTZT} are conformational compositions calculated from the DFT-based electronic energies E_{DFT}, E_{DFTZ}, and E_{DFTZT}, respectively.

TABLE 3: Structural Data for Compounds That Are the Most Similar to MDBL, As Retrieved from the Cambridge Structural Database

crystal structure[a]	space group[b]	abs config[c]	conformer[d]	Θ_{CSD}/deg[e]	Θ_{PM3}/deg[f]
DIVYIQ	$P2_1/c$	R	III	315.53	306.31
		S	I	44.47	53.69
DUXPOB[g]	$P-1$	R	III	300.32	311.24
		R	III	314.68	313.06
		S	I	59.68	48.76
		S	I	45.32	46.94
FUSHAC	$I2/c$	R	II	187.44	182.86
		S	II	172.56	177.14
NABXOD	$P2_1/n$	R	III	315.53	309.20
		S	I	44.47	50.80
TEYMOZ	$P2_1$	R	I	40.59	52.29
TICREC	$P2_12_12_1$	S	III	288.93	303.14
TOJHOP	$P2_1$	S	III	309.19	308.58
ULUYAB	$P2_1$	R	I	56.05	49.43
VOQROI	$P2_12_12_1$	R	III	52.02	51.40
ZUKYOT[g]	$P2_1$	S	III	304.48	310.03
		S	III	310.48	314.03

[a] Crystal structure represented by its CSD code. [b] Crystal symmetry expressed as the space group. Space groups with mirror or/and inversion symmetry operations allow packing of mirror-related isomers if the molecules do not lie on symmetry elements. [c] The absolute configuration at position 8′. [d] Conformers according to the convention adopted in Figure 4 for MDBL. [e] Experimental value of the torsion angle Θ (C1′−C7′−C8′−H8′), with H8′ crystallographically determined or modeled. [f] Value of the torsion angle Θ (C1′−C7′−C8′−H8′) as obtained from semiempirical geometry optimization of a crystallographically determined structure from the CSD. [g] Crystal structures with two chemically identical molecules in the asymmetric unit.

Packing effects on bond lengths and angles involving very heavy atoms like metals reach 0.02 Å and 2°, respectively, while for torsion angles they are in general much larger.[13] Strong hydrogen bonds and weak covalent bonds are practivally of the same strength.[67] Lignan lactones frequently have groups that form hydrogen bonds in the crystalline state. This reason could explain the difference between PM3-optimized and experimental torsion angles Θ ($\Delta\Theta$) for MDBL-like and HK-like structures

retrieved from the CSD. Previous works[24,56] have demonstrated that a good reproduction of bond lengths and hydrogen-bonding geometry requires *ab initio* or DFT methods, but it also depends on the initial geometry (number and relative position of molecules from the crystal structure). To explain the origin of the $\Delta\Theta$ deviation and find the methods which would minimize it, additional analyses have been carried out for the selected crystal structures related to MDBL and HK (Figures C−G and Tables C−F in the Supporting Information with comments and discussion). There are more experimental items that determine the $\Delta\Theta$: crystal determination quality and conditions (temperature, allotropic modification), the existence of more than one molecule in the asymmetric unit (different structural data for samples DUXPOB-1, DUXPOB-2, ZUKYOT-1, and ZU-KYOT-2 in Table C and AVOPIK-1 and AVOPIK-2 in Table E), crystal symmetry and molecular position with respect to the symmetry elements, disorder in the crystal, etc. The $\Delta\Theta$ deviation for ten MDL-like compounds (Table 3) is quantitatively correlated with some molecular and crystal properties (Figures D and E and Tables C and D), especially with the coordination number and numbers of strong interactions (correlation coefficients range from 0.43 to 0.78). This is due to the increase of molecular size and the presence of polar and hydrogen-bonding groups. It is difficult to select the computational approach that would be the best to reproduce experimental conformation of a MDBL-like molecule (Table G). Structure DIVJIQ[68] was selected for this analysis. Considering only the overal molecular conformation, the best results were obtained by molecular mechanics and even PM3 treatment of carefully selected molecular aggregates with strong intermolecular interactions. It is impossible to select a systematic high-level method that would be the best for all MDBL- and HK-like structures. Therefore, PM3 was used as an acceptable compromise between quality, simplicity, time, and appropriatness for qualitative comparison with crystal structures.

Figure 7 shows the results of computational conformational analysis at the PM3 level for conformer **I** by varying the C6′−C1′−C7′−C8′ angle. There are twins (**I−A, I−B**) and (**I−C,**

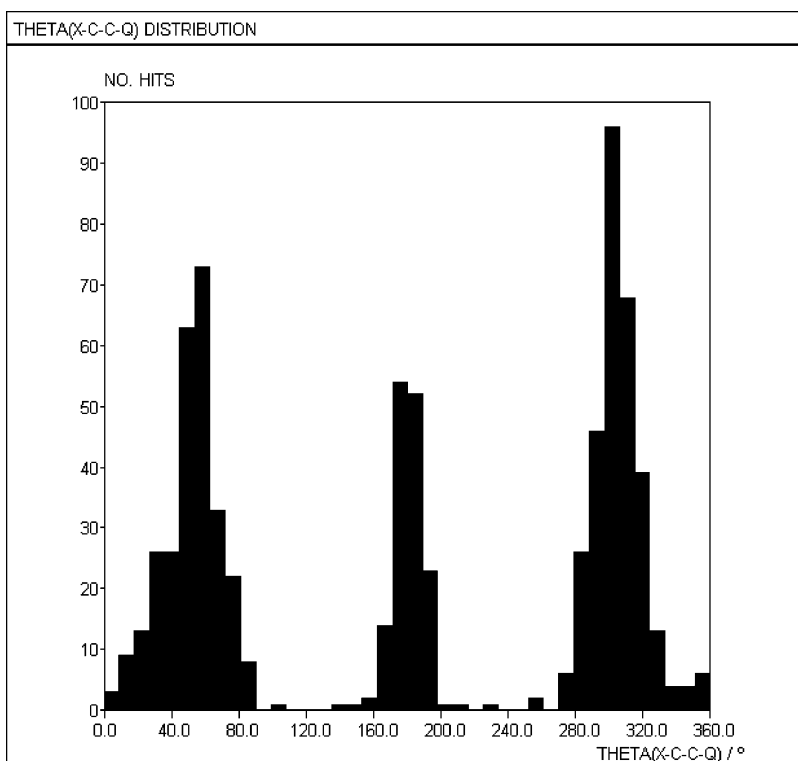**6322** *J. Phys. Chem. A, Vol. 111, No. 28, 2007*

Kiralj et al.

Figure 6. Histogram representation of torsion angle data for MDBL-like systems retrieved from the CSD, using the Vista program.
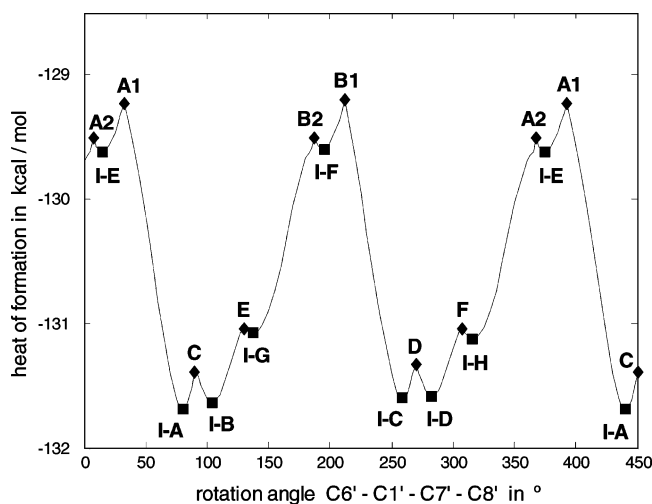

Figure 7. Heat of formation−rotation angle C6′−C1′−C7′−C8′ plot for MDBL from PM3 calculations. Several conformers (from **I**−**A** to **I**−**H**) and as well as rotation barriers (from **A1** to **F**) of different energies are visible. The original plot was extended from 360 to 450° for clarity.

I−**D**) that seem to interchange easily (barriers of 0.2−0.3 kcal mol^{-1}). Previous conformational analysis for MDBL around the C7′−C8′ bond resulted in conformer **I** which is in fact **I**−**B** in Figure 7, being only 0.06 kcal mol^{-1} above the global minimum **I**−**A**. The largest barriers are in the range 1.88−2.18 kcal mol^{-1}. Besides, the plot in Figure 7 is very symmetric due to the flatness of the aromatic system and small influences of the methylenedioxy ring even with adopted envelope conformation. Energy barriers **A1** and **B1** exist due to steric repulsions between hydrogen atoms of the phenyl ring (H2′ or H6′) and the lactone methylene hydrogens (both H8a and H8b) and γ-butyrolactone methylene hydrogens. However, DFT inspection of multiple minima and peaks in Figure 7 (geometry optimization without constraints) has shown clearly that minima and peaks in the regions around 90° and 270° fuse, while truncated peak profiles

around **A1** and **B1** become smooth. Again, the deficiency of the PM3 method is demonstrated by the artificial effect in multiplying conformers and barriers. The repetitive and symmetric profile of the plot in Figure 7 agrees well with the distribution of the analogous torsion angle that defines the position of phenyl ring relative to alkyl groups (Figure 8), as obtained by searching the CSD database (the searched fragment is defined in Figure H in the Supporting Information). Strong preference of the C−C bond to be positioned perpendicularly to the benzene ring is obvious in Figure 8. This is an intrinsic property of a benzene-like system attached to an alkyl group, confirmed by studies on simple prototype systems such as ethylbenzene,[69−72] propylbenzenes,[72] and butylbenzenes.[72−75] From the energetic point of view, the small difference between the conformers from the two angular regions (PM3, 0.091; DFT, 0.187 kcal mol^{-1}) can be a consequence of the aromatic system flatness and the fact that the C−H bond rotational barriers are very small (0.014 kcal mol^{-1} in toluene[76]). The C−C rotational barriers for ethylbenzene have been reported to be approximately 1 kcal mol^{-1} (0.7−1.3 kcal mol^{-1})[70,71] and similarly for *tert*-butylbenzene (1.1 kcal mol^{-1}).[75] These results indicate that the main contribution for the C1′−C7′ rotation barrier around the benzene ring in MDBL comes from H···H steric interactions between the benzene and γ-butyrolactone rings. The maximum difference between the highest barrier and the most stable conformer in Figure 7 (2.489 kcal mol^{-1}) is consistent with the DFT results (2.395 kcal mol^{-1}). When looking at the small data set of structures from the CSD, presented in Figure C in the Supporting Information and Table 3, one cannot see relationships between conformational preference (torsion angle types +g, −g, t) and the compound class: lactone, lactam, ketone, imine, amine, alcohol and substituted hydrocarbon in terms of the central 5-membered ring.

Computational and Structural Conformational Analysis for (—)-Hinokinin (HK). The results of the PM3 semiempirical conformational study for HK are shown in Figure 9. Nine

Conformational Study of Lignanolactones

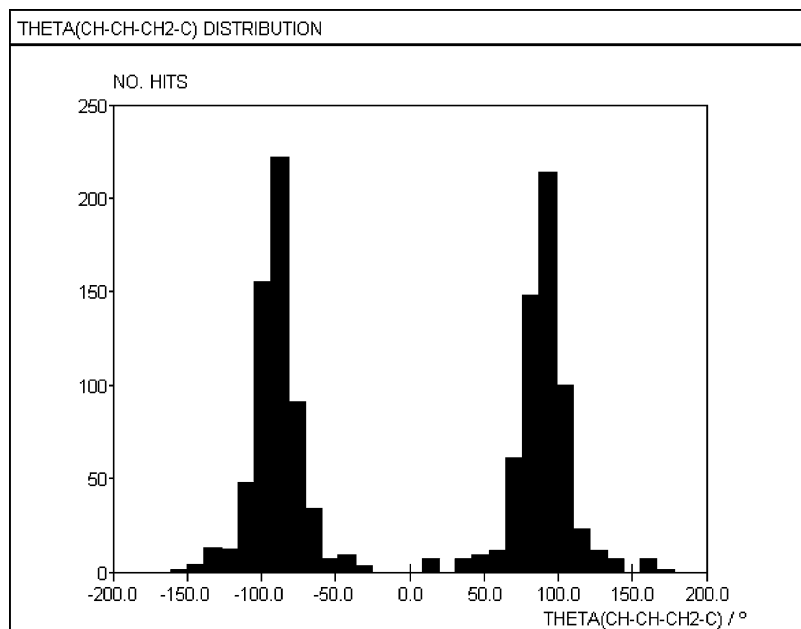*J. Phys. Chem. A, Vol. 111, No. 28, 2007* **6323**

Figure 8. Histogram representation of torsion angle data for phenyl−alkyl systems retrieved from the CSD, using the Vista program.

conformers were detected (**I**−**IX**) on the heat of formation−Θ_1−Θ_2 surface. Assuming that the rotations of the two methylenedioxybenzyl units around C7′−C8′ and C7−C8 bonds are rather independent, the present results are in accordance with those from the conformational study for MDBL where three conformers were detected. The nine conformers differ qualitatively in the relative position of the R or methylenedioxybenzyl units, as can be seen from geometric and energy parameters in Table 4. Using the terminology from (hetero)aromatic structural chemistry, the conformers can be characterized as follows: (a) stacked conformer[77,78] where the C_6 aromatic units are in nearly parallel and stacked relative position; (b) V-shaped or inclined conformer[79] with the aromatic groups possibly interacting in such a way that the planes of the aromatic rings make an acute angle (letter V), similar to T-shaped interaction of heteroaromatic rings[77,80] (distorted letter T); (c) extended conformer where the aromatic groups are certainly far from each other, separated by the γ-butyrolactone ring, so the molecule achieves its most extended form; (d) intermediate conformer where the aromatic groups are partially separated by the γ-butyrolactone ring but are still inclined toward each other as in a V-shaped conformer. Figure 10 illustrates these conformer types. One should note that the conformer classification given in Table 4 is valid for HK derivatives and analogues which are *trans*-(8α,8′β or 8β,8′α) and not for *cis*-analogues (8α,8′α or 8β,8′β).

The two rotations in HK cause various structural changes. The γ-butyrolactone ring adopts "up" conformation on C8′ in **I** and **VII** only, while in other conformers it has a "down" conformation. However, C8′ undergoes different deviations, ΔC8′, from the plane formed by the other four atoms. The planarity parameter Π for this plane also varies with the rotations, although there is no clear relationship between ΔC8′ and Π. The conformers can be well characterized by the closest contacts (2.4 Å for H···H contacts) including the three ring systems and two methylene spacers. The two R units never establish so close contacts (Ar···Ar in Table 4) that would inhibit each other's rotation. The main contributors to energy barriers are steric interactions C8′H₂···H₂C9′, C7H₂···O=C, and interactions between benzene hydrogens and the γ-butyrolactone ring (all hydrogens and the carbonyl oxygen).

There are 20 rotational barriers which exist between the HK conformers on the potential energy surface (Figure 9). Only two of them act as local maxima for two interconversions, while the other 18 are saddle (inflection) points with respect to Θ_1 or Θ_2. These points are positioned in the most probable pathways for conformer interconversions. The highest rotational barriers and saddle points are concentrated around values 120 and 240° for Θ_1 and Θ_2, as one would expect (staggered conformations). According to the rotation angle values, the conformers are distributed over all the conformational space (see Figure 9). The conformer energy differences range from 0.018 to 2.022 kcal mol⁻¹ as obtained from PM3 computations and from 0.091 to 2.080 kcal mol⁻¹ as resulting from various DFT energy correction schemes (Table 4). These ranges are greater than those for MDBL (Table 2), what is consistent with the differences between the chemical structures of HK and MDBL. Conformational composition from PM3 computations favors **III**, **IV**, and **VII** conformers (72%, Table 4) which are ±*g* in Θ_2. More precise DFT approaches give preference to **II**, **V**, and **VIII** (contributions ≥65%) which are *t* in Θ_2, while **III**, **IV**, and **VI** have always small contributions. The contributions for **I**, **VII**, and **IX** depend on the electron energy correction schemes. These three groups of conformers are visible as three distinct regions in the potential energy plot (Figure 9 left): linear (**VII**−**I**−**V**), left triangular (**VII**−**IX**−**I**), and right triangular (**III**−**VI**−**IV**) regions.

The stacked conformer **I**, due to its face-to-face π···π intermolecular interactions between the phenyl rings, is a special case with respect to all other conformers. For example, four steric parameters calculated by Chem3D,[39] Connolly accessible area, Connolly molecular area, Connolly solvent excluded volume and ovality are in linear or curvilinear mutual relationships for conformers **II**−**IX**. Conformer **I** either disrupts these regularities or behaves like an extrapolated point in the scatterplots (not shown). One can notice from Figure 10 that **I** is a relatively compact structure, with lower ovality (1.50) with respect to other conformers (1.52−1.57), smaller Connolly accessible area (456 Å²) than the other conformers (486−504 Å²), and a higher Connolly excluded volume (281 Å³) than in **II**−**IX** (265−270 A³). This shows that the behavior of **I** is

TABLE 4: Computational Conformational Summary for Conformers I−IX of HK

properties	I	II	III	IV	V	VI	VII	VIII	IX
molecular confm[a]	+g+g	+g−t	+g−g	−t+g	−t−t	−t−g	−g+g	−g−t	−g−g
description[b]	stacked	V-shaped	V-shaped	V-shaped	extended	V-shaped	intermediate	intermediate	extended
Θ_1[c]	48.88°/56.91°	52.66°/52.13°	51.33°/54.46°	185.86°/180.68°	188.06°/175.34°	187.85°/180.17°	310.00°/309.94°	309.10°/300.75°	308.82°/299.68°
Θ_2[c]	45.68°/55.48°	183.96°/177.35°	325.66°/330.04°	51.64°/60.00°	187.41°/175.14°	327.85°/340.26°	50.00°/56.26°	185.96°/177.36°	327.51°/333.68°
lactone confm[d]	"up"	"down"	"down"	"down"	"down"	"down"	"up"	"down"	"down"
ΔC8′/Å[e]	+0.408	−0.387	−0.475	−0.403	−0.492	−0.488	+0.468	−0.415	−0.526
Π/Å[f]	0.039	0.020	0.011	0.029	0.002	0.009	0.029	0.031	0.011
d(CH$_2$···H$_2$C)/Å[g]	≥ 2.427	≥ 2.476	≥ 2.470	≥ 2.922	≥ 2.918	≥ 2.967	≥ 2.834	≥ 2.511	≥ 2.547
d(CH$_2$···O=C)/Å[h]	≥ 2.794	≥ 2.696	≥ 2.836	≥ 2.617	≥ 2.714	≥ 2.724	≥ 2.814	≥ 2.734	≥ 2.781
d(ArH···HC)/Å[i]	≥ 2.519	≥ 2.821	≥ 2.507	≥ 2.516	≥ 2.667	≥ 2.515	≥ 2.687	≥ 2.985	≥ 2.768
d(ArH···O=C)/Å[j]	≥ 4.524	≥ 2.517	≥ 2.415	≥ 4.686	≥ 2.504	≥ 2.442	≥ 4.553	≥ 2.442	≥ 2.391
d(Ar···Ar)/Å[k]	≥ 2.710	≥ 2.926	≥ 3.058	≥ 2.864	≥ 4.150	≥ 2.937	≥ 4.579	≥ 3.604	≥ 5.574
E_{PM3}/kcal mol^{-1} [l]	−169.668	−169.650	−170.206	−170.027	−168.773	−169.170	−170.795	−169.547	−169.606
E_{DFT}/kcal mol^{-1} [m]	0.376	0	1.748	1.135	0.350	1.611	1.409	0.434	1.184
E_{DFTZ}/kcal mol^{-1} [m]	0.525	0	1.434	1.039	0.189	1.596	1.012	0.195	0.730
E_{DFTZT}/kcal mol^{-1} [m]	1.039	0.492	1.182	0.947	0.091	2.080	0.808	0	0.475
w_{PM3}[n]	6.51%	6.32%	16.15%	11.94%	1.44%	2.81%	43.65%	5.31%	5.87%
w_{DFT}[o]	17.34%	32.70%	1.71%	4.81%	18.11%	2.16%	3.03%	15.71%	4.44%
w_{DFTZ}[o]	11.26%	27.31%	2.43%	4.73%	19.85%	1.85%	4.95%	19.65%	7.97%
w_{DFTZT}[o]	4.89%	12.32%	3.84%	5.71%	24.23%	0.84%	7.23%	28.25%	12.67%

[a] Molecular conformation is defined by the position of the 3,4-methylenedioxybenzyl groups relative to the γ-butyrolactone ring, expressed as the rotation angle Θ_1 or H8′−C8′−C7′−C1′ and Θ_2 or H8−C8−C7−C1. [b] Conformer type according to the relative position of the methylenedioxybenzyl groups. [c] The values of Θ_1 and Θ_2 that were obtained from PM3/DFT (B3LYP 631G**) geometry optimization. [d] Conformation of the γ-butyrolactone ring is expressed as the envelope on C8′ which is turned "up" or "down" from the plane of the other four ring atoms, as obtained from the DFT calculations. These conformations are known in the literature under the names "bent axial" and "bent equatorial", respectively. The plane coincides with the plane of the paper when molecular formula of HK (Figure 2) is viewed. [e] Deviation of atom C8′ from the least-squares plane of the other four atoms of the γ-butyrolactone ring, as obtained from the DFT calculations. [f] Planarity parameter for the four atoms that define the least-squares plane of the γ-butyrolactone ring, defined as $\Pi = [\Sigma_i(\Delta_i)^2]^{1/2}$ where Δ_i is the deviation of a particular atom from the plane. [e] H···H distances between the C7′ methylene group and methylenes of the γ-butyrolactone ring, calculated for the DFT-based geometry. [g] H···H distances between the methylene groups C7′H$_2$ and C9′H$_2$, calculated for the DFT-based geometry. [h] H···O distances between C7H$_2$ and O=C groups. [i] H···H distances between the benzene rings and HC groups of the γ-butyrolactone ring. [j] H···O distances between the benzene ring at C7 and the O=C group. [k] H···H,C,O distances between the methylenedioxybenzyl groups. [l] Heat of formation from the PM3 geometry optimization. [m] Electronic energies relative to the most stable conformer, calculated from the DFT (B3LYP 6-31G**) geometry optimization: uncorrected electronic energy (E_{DFT}), electronic energy corrected for the zero-point energy (E_{DFTZ}) and electronic energy corrected both for the zero-point energy and thermal energies (translational, rotational, and vibrational at 298.15 K). [n] Conformational composition calculated from PM3-based heats of formation. [o] w_{DFT}, w_{DFTZ}, and w_{DFTZT} are conformational compositions calculated from the DFT-based electronic energies E_{DFT}, E_{DFTZ}, and E_{DFTZT}, respectively.

Conformational Study of Lignanolactones

J. Phys. Chem. A, Vol. 111, No. 28, 2007 **6325**
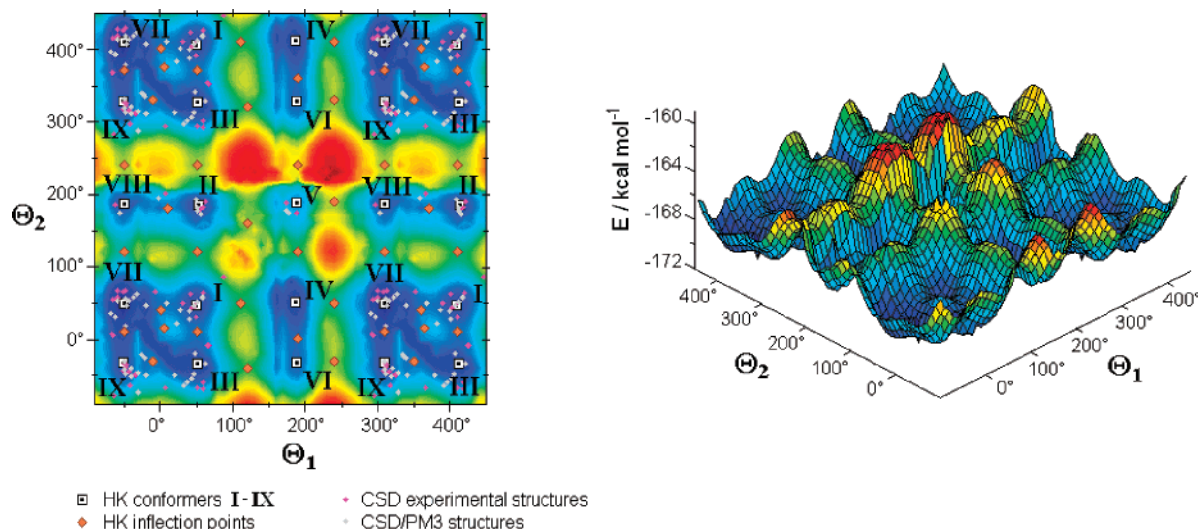
Figure 9. Results for the PM3 computational conformational analysis of HK represented as the heat of formation surface depending on the torsion angles Θ_1 (C1′−C7′−C8′−H8′) and Θ_2 (C1−C7−C8−H8). Left: The surface projected onto the Θ_1-Θ_2 plane and with detected conformers **I−IX**, 20 rotational barriers, crystal structure data from the Cambridge Structural Database and corresponding PM3-optimized data. The original plot was extended from −90 to +450° to facilitate the visualization of the relationships between the conformers and barriers. Right: 3D potential energy surface.

probably different from that of **II−IX** in intermolecular interactions in various chemical and biological systems.

Figure 4 represents the conformational properties of MDBL when the rotation of R is performed about the C7′−C8′ bond. The same bond and its approximate symmetry equivalent C7−C8 exist in HK. One can question how much this rotation affects the molecular energy. The plot of the heat of formation as a function of the rotation angle around the C1′−C7′ bond (from PM3 calculations, not presented) has basically the same shape as the analogous plot for MDBL (Figure 7), with the same number and relative position of all conformers and rotation barriers. Conformer **VII** appears only 0.18 kcal mol^{-1} above the global minimum conformer as obtained from PM3 computations. In fact, what was said about conformers obtained by rotation around the C1′−C7′ bond in MDBL also applies to this conformational analysis. The rotation of the aromatic groups around the C1′−C7′ bond does not affect significantly the other aromatic group. The rotation barrier peaks are in the range of 2.40−2.76 kcal mol^{-1}, being somewhat higher than the analogous barriers for MDBL. Structures of the corresponding conformations are characterized by steric repulsions between phenyl hydrogens (H2′ or H6′) and the lactone methylene hydrogens (H9′a and H9′b). The carbonyl oxygen is the main reason why the exact molecular symmetry cannot be C_2, and as a consequence, the heat of formation - rotation angle C6−C1−C7−C8 plot is different from the analogous plot for rotation around the C1′−C7′ bond (rotation angle C6′−C1′−C7′−C8′; plot not presented). Qualitatively, there is no great difference, as there are nine conformers and nine energy barriers in this new plot, with the largest barriers being in the range of 1.67−1.86 kcal mol^{-1}. The most apparent difference is that the distribution of the conformers along the rotation angle (rotation around the C1−C7 bond) is rather uniform. Furthermore, **VII** in the new plot is only 0.16 kcal mol^{-1} above the global energy minimum conformer, and there are close contacts between the carbonyl oxygen and the methylene hydrogens (H7a, H7b) in the rotation barrier structures.

The CSD data mining for HK-related compounds resulted in a relatively small set of structures of diverse nature (27 structures represented in Figure F in the Supporting Information). These compounds are divided into four main groups (Table 5): *trans-*
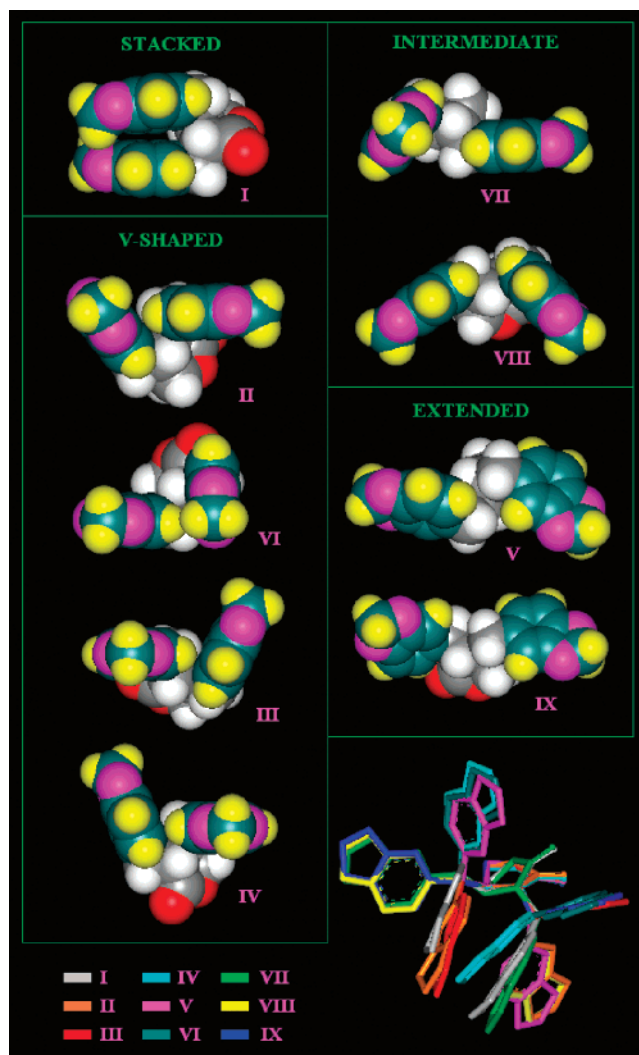
Figure 10. Nine HK conformers **I−IX** illustrated by space filling models where the methylenedioxybenzyl units are colored differently from the rest. The descriptive classification and the superimposition of the conformers (bottom) are also shown. Geometries are from DFT calculations.

TABLE 5: Structural Data for Compounds That Are the Most Similar to MDBL, As Retrieved from the Cambridge Structural Database

					angle/deg			
crystal structure[a]	space group[b]	ring config[c]	abs config[d]	conformer[e]	Θ_{1EXP}[f]	Θ_{1PM3}[g]	Θ_{2EXP}[f]	Θ_{2PM3}[g]
CEKVET	$P2_1$	*trans*	R,R	**II**	59.75	55.61	182.92	173.08
CEPTEW	$P2_1/n$	*trans*	R,R	**VII**	300.89	316.61	68.23	53.03
		trans	S,S	**III**	59.11	43.39	291.77	306.97
HXBZBL10	$P2_12_12_1$	*trans*	S,S	**II**	62.42	49.95	190.96	193.67
IKEHOV	$P2_1/c$	*trans*	R,R	**VII**	300.51	313.48	57.63	47.65
		trans	S,S	**III**	59.49	46.52	302.37	312.35
IVICIZ	$P2_12_12_1$	*trans*	R,R	**IX**	313.18	309.83	326.04	330.92
JIFKAK	Cc	*cis* (epimer 1)[h]	R,S	**Anti-I***	51.69	37.58	294.10	302.31
		cis (epimer 2)[h]	S,R	**Anti-I***	308.31	322.42	65.60	57.69
JIJJUH	$P2_1$	*trans* (epimer 1)[h]	R,R	**VII**	294.21	290.91	54.59	35.69
KIFLAM[i]	Fdd2	*trans*	R,R	**I**	86.99	47.40	86.99	47.40
QOQFEH	$P2_12_12_1$	*trans*	R,R	**VII**	312.80	311.37°	68.36°	57.38°
UBULOS	$P2_12_12_1$	*trans*	R,R	**IX**	295.95	311.40	283.27	313.54
VAWTUI	$P2_1/c$	*trans*	R,R	**II**	55.01	52.14	179.67	178.01
		trans	S,S	**II**	55.01	52.14	180.33	181.99
VEJBUH	$P2_1/c$	*cis*	R,S	V-shaped	41.44	39.93	63.49	39.46
		cis	S,R	V-shaped	318.56	320.07	296.51	320.54
DOHROH	$P2_12_12_1$	*trans* (epimer 1)[h]	S,S	**VII**	301.33	300.24	57.09	53.31
FAFYAM[i,j]	Fdd2	*trans*	R,R	**I**	46.38	52.10	46.38	52.10
XIHYUI[j]	$P2_1/n$	*trans* (epimer 1)[h]	R,R	**I−III** or **I−VII**	66.07	62.41	352.93	327.82
		trans (epimer 2)[h]	S,S	**III−IX** or **VII−IX**	293.93	297.59	7.07	32.18
IPILOS	$P2_1$	*trans* (epimer 1)[h]	R,S	**VIII**	298.20	303.57	185.64	174.17
JUFSIM[j]	$P2_12_12_1$	*trans*	R,R	**I**	50.45	28.12	31.33	41.07
NABGIH	$P2_1$	*trans*	S,S	**II−VII**	7.29	358.57	201.86	195.41
SOGDIB[j]	$P2_12_12_1$	*trans*	S,S	**IX**	326.67	319.38	311.18	310.47
VECRUQ[i,j]	C2/c	*trans*	S,S	**Anti-I***	48.81	58.83	48.81	58.04
YIHKAB[j]	$P2_1$	*trans* (epimer 1)[h]	S,S	**V**	174.88	177.32	174.88	173.96
AVOPIK	$P2_1$	*cis* (epimer 1)[h]	R,S	none	311.78	329.53	322.69	314.29
		cis (epimer 2)[h]	R,S	none	309.21	341.09	317.23	311.14
BUZBED	$P2_12_12_1$	*trans*	R,R	none	325.89	329.00	311.98	287.05
ETAREW[j]	P−1	*trans* (epimer 1)[h]	R,R	none	7.32	19.22	293.46	312.14
		trans (epimer 2)[h]	S,S	none	352.68	340.78	66.54	47.86
MANGEO	$P2_12_12_1$	*trans* (epimer 1)[h]	R,S	none	60.06	8.62	65.17	49.78
QAJFAJ	$P2_1/n$	*trans*	R,R	none	317.03	337.76	316.33	337.26
		trans	S,S	none	42.97	22.24	43.67	22.74
TAJDIR[j]	C2	*trans*	S,S	none	313.34	334.79	325.64	339.60

[a] Crystal structures represented by their CSD codes and divided into four groups: lignano lactones (first group, 12 structures), other related lignans (second group, three structures), and other related compounds that are topologically similar to lignano lactones (third group, six structures with two planar C_5 or C_6 ring units; fourth group, six structures with one or two nonplanar C_5 or C_6 ring units). [b] Crystal symmetry expressed as the space group. Space groups with mirror or/and inversion symmetry operations allow packing of mirror-related isomers if the molecules do not lie on symmetry elements. [c] The γ-butyrolactone, tetrahydrofuran, cyclohexane or other five-membered central ring conformation at positions 8 and 8′: 8,8′-aromatic units are either in *cis*- or *trans*- positions, i.e., they are on the same or opposite sides of the five-membered central ring, respectively. [d] The absolute configuration at positions 8 and 8′. [e] Conformers of *trans*-compounds, according to the convention adopted in Table 4 for HK. The conformers of the two *cis*-compounds are anti-stacked (JIFKAK) and V-shaped (VEJBUH) instead of **III/VII** and **I/IX** as for *trans*-compounds, respectively. Some conformers are intermediates between two neighboring HK conformers. **Anti-I*** is anti-stacked conformer, in which substituents at C8 and C8′ sterically hinder the C_6 aromatic ring units to adopt positions for the stacking conformer. To the fourth group of structures none of the conformers **I−IX** can be attributed. [f] Experimental value of the torsion angles Θ_1 (C1′−C7′−C8′−H8′) and Θ_2 (C1−C7−C8−H8), with H8′ and H8 crystallographically determined or modeled. [g] Value of the torsion angles Θ_1 (C1′−C7′−C8′−H8′) and Θ_2 (C1−C7−C8−H8) as obtained from semiempirical geometry optimization of a crystallographically determined structure from the CSD. [h] Isomers with additional chiral centers (two or more epimers). [i] Molecule situated on a 2-fold rotation axis. [j] Structures with alternative choice for angles Θ_1 and Θ_2 due to the C_2 symmetry of the central ring (see Figure F in Supporting Information).

(10 structures) and *cis*-lignan lactones (structures JIFKAK and VEJBUH), other analogue *trans*-lactones (structures DOHROH, FAFYAM and XIHYUI), *trans*-analogues of lignan lactones with both ring units planar (six structures), and other compounds topologically similar to lignan lactones but with one or both ring units essentially nonplanar (six structures). The conformers of the first three groups with exception of the *cis*-compounds may be classified as HK conformers **I−IX** or their intermediates. The two possibilities of choice of angles Θ_1 and Θ_2 for eight molecules with orientational ambiguity of the symmetrical central ring, was also taken into account (see Table 5). Four retrieved structures are of organometallic compounds, from which two have planar ring units (JUFSIM and SOGDIB) and two have nonplanar rings (BUZBED and QAJFAJ).

The experimental and PM3 torsion angle data (Table 5), taking into account the orientational ambiguity for some molecules, were placed in the Θ_1-Θ_2 conformational space of HK (Figure 9 left). Although this torsion angle data set cannot ensure certain statistical weight as the large data set for MDBL-like compounds (Figure 8), some trends are rather visible and though worth to mention. All torsion angles concentrate around the positions for seven from nine HK conformers (**I−III**, **V**, and **VII−IX**) or among these positions in the valley regions (colored blue in Figure 9 left) with negligible energy barriers within them. The PM3 data are in general less dispersed than the experimental data set, due to the crystal packing effects that are absent in the PM3 data set and because of reasonable differences between the two data sets (ranging from modest differences to 51°, Table 5). Such trends have been already

Conformational Study of Lignanolactones

J. Phys. Chem. A, Vol. 111, No. 28, 2007 **6327**

TABLE 6: Calculated[a] Vicinal H−H Coupling Constants (Hz) for MDBL

equation[b]	^3J(H7'a−H8')				^3J(H7'b−H8')			
	PM3	DFT	DFTZ	DFTZT	PM3	DFT	DFTZ	DFTZT
HLA equation (chemical groups)[c]	6.5	7.5	7.7	7.8	7.3	7.0	6.9	7.1
DAD equation[c]	6.5	7.4	7.7	7.8	7.2	7.0	6.9	7.0
DAD equation (cross terms)[c]	6.4	7.4	7.6	7.7	7.2	6.9	6.8	7.0
CJG equation[c]	8.4	9.7	10.0	10.1	9.5	9.0	8.8	9.0
HLA equation general[c]	7.1	8.3	8.6	8.6	8.0	7.6	7.5	7.7
HLA equation (general, β-effects)[c]	7.0	8.2	8.5	8.5	7.9	7.5	7.4	7.6
HLA equation (two substituents)[c]	7.1	8.3	8.7	8.7	8.1	7.7	7.5	7.7
HLA equation (three substituents)[c]	6.8	7.9	8.2	8.3	7.7	7.3	7.2	7.4
HLA equation (four substituents)[c]	6.7	7.9	8.2	8.3	7.7	7.3	7.2	7.4
Karplus equation[c]	5.4	6.2	6.4	6.4	6.1	5.7	5.7	5.8
HLA equation (Barfield effect)[c]	6.1	7.0	7.2	7.3	6.7	6.6	6.5	6.6
HLA equation[d]	6.3	7.3	7.5	7.6	7.1	6.8	6.7	6.9
average (std dev)[e]	6.7(7)	7.8(9)	8.0(9)	8.1(9)	7.5(9)	7.2(8)	7.1(7)	7.3(8)

[a] Conformer fractions from Table 2: semiempirical distribution w_{PM3} (PM3), uncorrected DFT distribution w_{DFT} (DFT), DFT distributions corrected to the zero-point energy w_{DFTZ} (DFTZ) and thermal energies w_{DFTZT} (DFTZT). [b] Several equations used to calculate vicinal H−H coupling constants for conformers **I**−**III** of MDBL. These calculated values were averaged by molar fractions of the conformers. The abbreviations have the following meanings: HLA, Haasnoot−de Leeuuw−Altona; DAD, Díez−Altona−Donders; CJG, Colucci−Jungk−Gandour equations. [c] Calculations performed by using software MetRe-J.[20] [d] Calculation performed by using an online software.[58] [e] Average and standard deviation of all calculations.

noticed for the selected MDBL-like structures (Figure 4, Table 3). Crystal packing descriptors (Tables E and F; Figure G) show linear and nonlinear correlations with $\Delta\Theta$ for HK-like compounds, similarly to MDBL-like compounds. Hydrogen bonds and molecular size again play important role. On the basis of Figure 9, left, one may expect that other HK-like compounds that would be retrieved from the CSD in future, would group around **I**−**IX** or among these positions in the blue valleys. These new compounds would have five-membered rings as defined in Scheme A in the Supporting Information (containing other nonmetal elements besides carbon), and two general ring units with sp² or sp³ carbon spacer between them and the central ring. Similar generalizations were showed to be realistic for MDBL compounds (Figure 6).

More detailed analysis of torsion angle data in Figure 9 left shows possible preferences for some compound types to group in certain regions of the Θ_1−Θ_2 space. Most *trans*-lignans tend to concentrate around V-shaped conformers (**II**, **III**) and intermediate (**VII**) conformers, *cis*-lignans do not show any preference, other compounds with planar ring units group around **I** (stacked and anti-stacked conformers) and **IX** (extended), and compounds with nonplanar rings are dispersed in the large valley of the four conformers (**I**, **III**, **VII**, and **IX**). All lignans are grouped in this valley and also around conformer **II**. However, the set HK-like compounds is too small for statistical evaluation of the HK conformers preference in chemical and biological systems.

Computed-NMR Conformational Analysis for MDBL and HK. Experimental vicinal proton−proton coupling constants for the protons at C7' and C7 were compared to the values calculated from torsion angles of PM3- and DFT-based geometry for MDBL (Tables 6 and 7) and for HK (Tables 8−10).

MDBL has three conformers with the group R (3,4-dimethyleneoxyphenyl) in position −*g* (**I**), *t* (**II**), and +*g* (**III**) with respect to H8'. Various computational procedures to calculate vicinal coupling H−H constants from corresponding torsion angles have resulted in values in the ranges 5.4−10.1 and 5.7−9.5 Hz for H7'a and H7'b protons, respectively. Experimental coupling constants (Table 7) have very small variations (standard deviations 0.1 and 0.3 Hz) and distinguish the two protons (the average values differ by 1.1 Hz). According to PM3 and DFT computations, protons H7'a and H7'b (Table 6) are protons with higher and lower coupling constants determined experimentally[81−93] (Table 7), respectively. When the average values

TABLE 7: Experimental Vicinal H−H Coupling Constants (Hz) for MDBL

reference	$^3J_1$	$^3J_2$
Honda et al.[81]	7.9	6.7
Bode et al.[82]	8.0	6.8
Sakakibara et al.[83]	8.0	6.8
Takekawa et al.[84]	8.2	6.8
Itoh et al.[85]	7.8	6.7
Brinksma et al.[86]	8.0	7.0
Vanderlei et al.[87]	8.0	7.9
Srikrishna et al.[88]	8.0	6.8
Morimoto et al.[89]	7.9	6.9
this work	7.7	6.8
this work[a]	8.1	6.8
average (std dev)[b]	8.0(1)	6.9(3)

[a] Measured in benzene-d_6. All other measurements were carried out in CDCl₃ or CHCl₃. [b] Average and standard deviation of all measurements.

standard deviations of experimental and computed coupling constants are compared, it is noticeable that DFT approaches produce better results than PM3 (maximum difference between the experimental and calculated average values is 0.4 for DFT and 1.3 for PM3). Among particular equations applied to calculate the vicinal coupling constants, Haasnot−Leeuuw−Altona and Díez−Altona−Donders equations give reasonable results, while the Karplus equation underestimates and Colucci−Jungk−Gandour equation overestimates the coupling constants predictions.

Experimental coupling constants for HK (Table 10) show greater differences between the "a" and "b" protons (1.8−1.9 Hz) than the experimental values for MDBL (Table 7). This has as a consequence larger interval (3.7−11.3 Hz) inside which the calculated coupling constants for HK are concentrated. Comparing the experimental values for MDBL and HK, it is visible that $^3J_{HH}$ values for C7H₂ are lower than those for C7'H₂ in both MDBL and HK. The presence of the carbonyl oxygen in the vicinity of the R group in HK may be the main reason for this phenomenon (see H···O=C distances in Table 4). Higher and lower experimentally determined coupling constants from literature[81−93] (Table 10) probably account for H7a and H7b protons, respectively (see average values in Tables 8 and 9), with relatively great variation for one of them. Until recently, the literature has not reported the coupling constant values for protons H7'a/H7'b. The measurements obtained in this and a recent work[93] clearly show that these $^3J_{HH}$ constants are greater

TABLE 8: Calculated[a] Vicinal H−H Coupling Constants (Hz) for HK (H7′a,b−H8′ Interactions)

	^3J(H7′a−H8′)				^3J(H7′b−H8′)			
equation[b]	PM3	DFT	DFTZ	DFTZT	PM3	DFT	DFTZ	DFTZT
HLA equation (chemical groups)[c]	7.8	5.2	6.1	7.8	5.4	8.0	6.9	5.1
DAD equation[c]	7.8	5.1	6.1	7.8	5.4	7.9	6.9	5.0
DAD equation (cross terms)[c]	7.7	5.1	6.0	7.7	5.3	7.9	6.8	5.0
CJG equation[c]	10.3	6.5	7.9	10.2	7.2	10.4	9.0	6.4
HLA equation general[c]	8.7	5.3	6.6	8.8	5.7	8.9	7.6	5.2
HLA equation (general, β-effects)[c]	8.6	5.3	6.5	8.6	5.6	8.8	7.5	5.2
HLA equation (two substituents)[c]	8.8	5.3	6.6	8.8	5.7	9.0	7.7	5.2
HLA equation (three substituents)[c]	8.4	5.1	6.3	8.4	5.4	8.6	7.3	5.0
HLA equation (four substituents)[c]	8.4	5.1	6.3	8.4	5.4	8.6	7.3	5.0
Karplus equation[c]	6.5	4.3	5.1	6.4	4.4	6.6	5.8	4.2
HLA equation (Barfield effect)[c]	7.3	5.1	5.9	7.4	5.2	7.4	6.6	5.0
HLA equation[d]	7.8	5.0	5.9	7.6	5.2	7.7	6.7	4.9
average (std dev)[e]	8.1(9)	5.2(5)	6.3(6)	8.2(9)	5.5(6)	8.3(10)	7.2(8)	5.1(5)

[a] Conformer fractions from Table 4: semiempirical distribution w_{PM3} (PM3), uncorrected DFT distribution w_{DFT} (DFT), DFT distributions corrected to the zero-point energy w_{DFTZ} (DFTZ) and thermal energies w_{DFTZT} (DFTZT). [b] Several equations used to calculate vicinal H−H coupling constants for conformers **I−IX** of HK. These calculated values were averaged by the molar fractions of the conformers. The abbreviations stand for the following: HLA, Haasnoot−de Leeuuw−Altona; DAD, Díez−Altona−Donders; CJG, Colucci−Jungk−Gandour equations. [c] Calculations performed by using software MetRe-J.[20] [d] Calculation performed by using an online software.[58] [e] Average and standard deviation of all calculations.

TABLE 9: Calculated[a] Vicinal H−H Coupling Constants (Hz) for HK (H7a,b−H8 Interactions)

	^3J(H7a−H8)				^3J(H7b−H8)			
equation[b]	PM3	DFT	DFTZ	DFTZT	PM3	DFT	DFTZ	DFTZT
HLA equation (chem groups) [HLAcg][c]	4.4	4.5	4.8	5.1	8.8	4.8	4.3	3.8
DAD equation [DAD][c]	4.4	4.5	4.8	5.1	8.7	4.8	4.3	3.8
DAD equation (cross terms) [DADct][c]	4.3	4.4	4.7	5.0	8.7	4.7	4.2	3.7
CJG equation [CJG][c]	5.6	5.3	5.7	6.2	11.3	6.2	5.6	4.9
HLA equation general [HLAg][c]	4.2	4.3	4.7	5.1	9.6	5.0	4.4	3.7
HLA equation (general, β-effs.) [HLAb][c]	4.2	4.3	4.7	5.0	9.5	4.9	4.3	3.7
HLA equation (two substituents) [HLA2s][c]	4.2	4.3	4.7	5.1	9.7	5.0	4.4	3.7
HLA equation (three substituents) [HLA3s][c]	4.0	4.1	4.4	4.8	9.3	4.7	4.1	3.5
HLA equation (four substituents) [HLA4s][c]	4.0	4.3	4.6	4.9	9.2	4.7	4.2	3.5
Karplus equation [KE][c]	3.7	3.6	3.8	4.1	7.1	4.1	3.8	3.4
HLA equation (Barfield effect) [HLABe][c]	4.1	4.5	4.7	5.0	7.7	4.8	4.4	3.9
HLA equation [HLA2][d]	4.1	4.1	4.3	4.7	8.3	4.6	4.1	3.6
average (std dev)[e]	4.3(4)	4.4(4)	4.7(4)	5.0(5)	9.0(11)	4.9(5)	4.3(4)	3.8(4)

[a] Conformer fractions from Table 4: semiempirical distribution w_{PM3} (PM3), uncorrected DFT distribution w_{DFT} (DFT), DFT distributions corrected to the zero-point energy w_{DFTZ} (DFTZ) and thermal energies w_{DFTZT} (DFTZT). [b] Several equations used to calculate vicinal H−H coupling constants for conformers **I-IX** of HK. These calculated values were averaged by the molar fractions of the conformers. The abbreviations stand for the following: HLA, Haasnoot−de Leeuuw−Altona; DAD, Díez−Altona−Donders; CJG, Colucci−Jungk−Gandour equations. The abbreviations in square brackets are those used in chemometric analysis (Figure 12). [c] Calculations performed by using software MetRe-J.[20] [d] Calculation performed by using an online software.[58] [e] Average and standard deviation of all calculations.

TABLE 10: Experimental Vicinal H−H Coupling Constants (Hz) for HK

reference[a]	$^3J_1$ (C7)	$^3J_2$ (C7)	$^3J_1$ (C7′)	$^3J_2$ (C7′)
Souza et al.[90]	7.3	5.1		
Honda et al.[81]	6.7	4.9		
Morimoto et al.[89]	6.9[c]	4.8[c]		
Morimoto et al.[89]	6.9[d]	5.0[d]		
Rehnberg et al.[91]	7.1	4.9		
Belletire et al.[92]	4.9	4.9		
Heleno et al.[93]	7.1	5.0	8.2	5.8
this work	7.3	5.1	8.6	7.1
average (std dev)[b]	6.8(7)	5.0(1)	8.4(2)	6.5(7)

[a] Coupling constants for methylene protons at C7 and C7′. [b] Average and standard deviation of all measurements (carried out in CDCl₃). [c] Racemic mixture. [d] (+)-Hinokinin.

than those for H7a/H7b. Unlike computational results for MDBL in terms of average $^3J_{HH}$ values (Table 6), the superiority of DFT methods over PM3 is not so visible from the results for HK (Tables 8 and 9). This difference between MDBL and HK can be a consequence of solvent effects, i.e., solvent−solute interactions.

It is known that solvent effect can significantly affect $^3J_{HH}$ constants and conformational composition of various organic compounds.[94,95] CDCl₃ and CHCl₃ were the solvents used in most determinations of experimental $^3J_{HH}$ values (Tables 7 and 10) while C₆D₆ was used only once (Table 7). Numerous organic compounds are characterized by similar solvation energies when dissolved in chloroform and benzene.[96,97] Besides, chloroform forms hydrogen bonds with oxygen-containing groups in the gas phase,[98,99] liquid,[100,101] and crystal,[102] the energy of which has been reported to be 2−6[98,102] kcal mol⁻¹, which is comparable to the rotation energy barriers in this work. Many amphiphilic compounds are characterized by similar solvation energies even when dissolved in water and chloroform,[96,103] mainly due to hydrogen bonding and polar interactions with the solvents. This fact justifies the calculation of aqueous solvation (hydration) energies of all conformers of MDBL and HK at DFT level, by means of the SM5.4 method of Truhlar et al.[104] which is implemented in the Titan software. The solvation energies for MDBL conformers show small variations (from −10.320 to −10.931 kcal mol⁻¹) while those for HK conformers vary more (from −12.629 to −15.495 kcal mol⁻¹). These variations, when presented as hydration energy relative to the most stable conformer (E_{solv}), show very interesting behavior when plotted against the DFT electronic energy (E_{DFTZT}), as shown in Figure 11 for HK conformers. There are three distinct

Conformational Study of Lignanolactones

J. Phys. Chem. A, Vol. 111, No. 28, 2007 **6329**

Figure 11. Solvation energy (E_{solv}) plotted against electronic energy corrected to the zero-point and thermal energies (E_{DFTZT}), relative to the most stable conformer of HK as obtained from DFT calculations. Numbers in brackets are average O···O distances in atomic units.

Figure 12. PCA scores for the $^3J_{HH}$ data set with data colored according to the methods by which they were obtained.

groups of conformers that demonstrate the increase of the hydration energy with conformer stability: the stacked **I**, the conformer **VI** that has rings in close contacts (Figure 10), and the rest positioned along a line (correlation coefficient between the two energies is 0.941). According to experimental hydration energies of oxygen-containing compounds,[104] the major contributors to the energy are carbonyl and ether oxygens in HK. In conformers **I** and **VI** these groups are concentrated in a relatively small space (see the previous discussion about the stacked conformer **I** and its shape parameters) and the molecules have such a shape that the possibility of formation of hydrogen or polar interactions with water or chloroform molecules is rather reduced. This situation corresponds to somewhat smaller average O···O distances, as illustrated in Figure 11.

Thus, HK has two conformers with four principal rotation angles which contribute to more obvious deviation from the main trend in Figure 11. This may explain why even DFT calculations were not so successful in predicting $^3J_{HH}$ values for HK as they were for those of MDBL. The fact that solvation favors more stable conformers can indicate that HK in biological systems (which contain water as the solvent) will be conformationally predetermined. According to Figure 11, MDBL will consist predominantly of **I** and **III** with 90% molar fraction (Table 2). HK will consist mainly of **V** (extended) and **VIII** (intermediate) with 52% fraction, and in significaqnt extent of **II** (V-shaped with a C−H···π interaction) and **IX** (extended) with 25% fraction (Table 4). These are therefore, the most probable candidates for bioactive conformers of HK.

Experimental and computed $^3J_{HH}$ data from Tables 6−10 were organized into a matrix with dimensions 52 × 6. The six columns (variables) are the coupling constants for the two methylene protons in MDBL (H7′a and H7′b) and four in HK (H7′a, H7′b, H8′a and H8′b). The samples are 48 computational (12 equations × four approaches: PM3 and three DFT approaches) and 4 experimental (two from this work, Exp-tw-I and Exp-tw-II, and two as averages of literature data, Exp-av-I and Exp-av-II) methods. The experimental methods "I" account for data as presented in Tables 6−10, assuming that "a" and "b" protons have higher and lower $^3J_{HH}$ values, respectively. The experimental methods "II" account for the opposite coupling constant assignment to these methylene protons.

The basic abbreviations of the methods are given in Table 9. The data compression in the PCA (Figure 12) shows that the first three principal components (PCs) contain 92% of the total

variance (PC1: 41%, PC2: 31%, PC3: 20%). The four approaches (PM3 and three DFT) for calculation of coupling constants occupy distinct regions of the scores space. KE or Karplus equation-based and CJG-based methods are placed farthest from the experimental methods. PC3 distinguishes well the "I" from "II" experimental methods, where the former are generally closer to computational methods than the latter. The five closest DFTZT methods with HLA equations (HLAb, HLAg, HLA2s, HLA3s, and HLA4s, see Table 9) can be considered as the best choices for calculation of $^3J_{HH}$ constants for the protons at C7′ and C7 in MDBL and HK. It is noticeable that the PCA analysis confirms previous observations in favor for the methods "I" as the correct assignment for methylene protons, according to which "a" and "b" protons have higher and lower vicinal coupling constants, respectively.

4. Conclusions

Computational and experimental studies applied to conformational properties of lignano-9,9′-lactones, in particular to hinokinin HK and its precursor MDBL, lead to the following conclusions.

(1) The lignano-9,9′-lactone precursor MDBL possesses three conformers that correspond to three conformer types ($-g$, t, $+g$) with differences around 1 kcal mol^{-1}. $^3J_{HH}$ coupling constants for methylene protons at C7′, based on DFT geometry, are fairly well calculated, as expected.

(2) Lignano-9,9′-lactones are semiflexible systems with at least four rotational degrees of freedom and energy barriers below 5 kcal mol^{-1} that enable considerable rotation of the aromatic C_6 ring units with respect to the γ-butyrolactone ring.

(3) Four conformer types of *trans*-lignano-9,9′-lactones exist in the crystal state as well as in vacuum: stacked, V-shaped, intermediate, and extended, defining the relative positive of the C_6 ring units.

(4) Nine conformers, with energy differences of 2 kcal mol^{-1}, were detected for HK. DFT geometry of these conformers allows rather approximate calculation of $^3J_{HH}$ coupling constants for methylene protons at C7′ and C7, with pronounced solvent effects such as hydrogen bonds.

(5) The best methods for calculation of the coupling constants, as observed by using PCA, are B3LYP 6-31G** calculations with zero-point and thermal energy corrections, coupled with some variants of the Haasnoot−de Leeuuw−Altona equations.

(6) Higher and lower values of the vicinal coupling constants correspond to methylene protons designated as H7a/H7′a and H7b/H7′b, respectively, as confirmed from various calculation methods and PCA. Protons H7a and H7b have lower coupling constants than H7′a and H7′b probably due to the interaction of the carbonyl oxygen with the neighboring phenyl ring.

(7) Rotation of substituted phenyl rings (C$_6$ units) around the C7′−C8′ and C7−C8 bonds is the main determinant of conformational properties of *trans*-lignano-9,9′-lactones with small substituents on these rings. The rotation around the C1′−C7′ and C1−C7 bonds has barriers less than 3 kcal mol^{-1}.

(8) Data mining in the Cambridge Structural Database has shown a fair agreement with computed conformational analysis for the both compounds, enabling generalization for topologically similar systems. Difficulties in reproducing experimental conformation of such compounds lies in crystal packing effects that determine the molecular conformation in the solid state, in particular, hydrogen bonds.

(9) The most stable conformers of MDBL (90% molar fraction: **I** and **III**) and HK (77% molar fraction: **II**, **V**, **VIII**, and **IX**) are expected to have important role in chemical and biological systems. Hydration favors more stable HK conformers.

5. Experimental Section

General Data. All ^{1}H and ^{13}C NMR spectra were recorded at 300 and 75 MHz, respectively, using a Bruker DPX-300 instrument and chloroform-*d* (CDCl$_3$) or benzene-*d$_6$* as solvent; chemical shifts are in ppm downfield from tetramethylsilane internal standard. IR spectra were measured with a Perkin-Elmer Spectrum RX IFTIR System, and the most intense or representative bands are reported (in cm^{-1}). TLC was performed on plates precoated with silica gel 60 F$_{254}$ (0.25 mm thick, Merck) and column chromatography separations were performed with silica gel 60 (70−230 mesh, Merck). Melting points were determined on a Reichert Kofler block apparatus and are uncorrected.

4-(3′,4′-Methylenedioxyphenyl)-3-methoxycarbonyl-3-butenoic Acid (3). Metallic sodium (2.7601 g, 0.12 mol) was dissolved in anhydrous methanol (40 mL) under inert atmosphere at reflux temperature. A solution of dimethylsuccinate (**2**) (11.1066 g, 0.076 mol) and piperonal (**1**) (21.3005 g, 0.106 mol) in anhydrous methanol (15 mL) were added. The reaction was monitored by TLC, and after 5 h under reflux the reaction mixture was cooled and acidified with 6 M HCl. The methanol was evaporated under reduced pressure and the resulting mixture was diluted with dichloromethane. The aqueous layer was extracted with dichloromethane and the combined organic extracts were washed with water, brine and dried over anhydrous magnesium sulfate. After evaporation of solvent under reduced pressure, the yellow residue was recrystallized from methanol to give compound **3** (14.8702 g, 0.057 mol, 75%): mp 150−151 °C. ^{1}H NMR (CDCl$_3$): δ 7.82 (s, 1H), 6.93 (dd, J = 1.9, 8.1 Hz, 1H), 6.89 (d, J = 1.9 Hz, 1H), 6.79 (d, J = 8.1 Hz, 1H), 6.0 (s, 2H), 3.83 (s, 3H), 3.59 (s, 2H). ^{13}C NMR (CDCl$_3$): δ 176.4 (C1), 168.1 (C5), 148.5 (C5′), 148.5 (C4′), 142.4 (C4), 124.0 (C1′), 123.6 (*C2′*), 109.1 (C3′), 108.6 (C6′), 101.4 (C7), 96.1 (C3), 52.4 (C6), 33.6 (*C2*). IR (cm^{-1}): 820 (C−H, Ar), 1026−1255 (C−O), 1443−1517 (C=C), 1708 (C=O), 3420 (O−H).

4-(3′,4′-Methylenedioxyphenyl)-3-methoxycarbonylbutanoic Acid (4). A solution of compound **3** (5.0031 g, 18.9 mmol) in methanol (25 mL) was hydrogenated under 20 atm of H$_2$ at room temperature with a catalyst containing 5% palladium on activated carbon powder (0.2005 g). After 24 h under agitation,

the catalyst was removed by filtration through Celite and the solvent was evaporated under reduced pressure. The residue was purified by recrystallization from methanol to afford **4** (4.5369 g, 17.0 mmol, 90% yield) as a white solid: mp 103−105 °C. ^{1}H NMR (CDCl$_3$): δ 6.72 (d, J = 7.8 Hz, 1H), 6.64 (d, J = 1.6 Hz, 1H), 6.59 (dd, J = 7.8, 1.6 Hz, 1H), 5.93 (s, 2H), 3.68 (s, 3H), 3.01−3.08 (m, 1H), 2.97 (dd, J = 13.0, 6.0 Hz, 1H), 2.70 (dd, J = 13.0, 9.0 Hz, 1H), 2.67 (dd, J = 17.0, 9.0 Hz, 1H), 2.45 (dd, J = 17.0, 5.0 Hz, 1H). ^{13}C NMR (CDCl$_3$): δ 177.4 (C1), 174.4 (C5), 147.8 (C5′), 146.4 (C4′), 131.6 (*C2′*), 122.0 (C1′), 109.2 (C3′), 108.3 (C6′), 100.9 (C7), 52.0 (C6), 42.9 (C3), 37.3 (C4), 34.5 (*C2*). IR (cm^{-1}): 816 (C−H, Ar), 1084, 1245 (C−O), 1515, 1533 (C=C Ar), 1699, 1735 (C=O), 3452 (O−H).

(3′,4′-Methylenedioxybenzyl)-γ-butyrolactone (MDBL) (5). A drop of phenolphthalein and KOH (0.1456 g, 2.6 mmol) were added to a stirred solution of compound **4** (0.7112 g, 2.6 mmol) in absolute ethanol (15 mL) at room temperature. After completing the reaction, CaCl$_2$ (0.6920 g, 6.2 mmol) and absolute ethanol (50 mL) were added. The suspension was cooled to −10 °C and a solution of NaBH$_4$ (0.3735 g, 9.9 mmol) in absolute ethanol (30 mL) was added dropwise. The mixture was stirred at room temperature for 5 h, then cooled to 0 °C and acidified with 6 M HCl. After 15 min of agitation, distilled water was added until the solution become clear and the ethanol was evaporated under reduced pressure. The aqueous layer was extracted with dichloromethane, and the organic extract was washed with water and dried over anhydrous magnesium sulfate. The solvent was evaporated under reduced pressure and the residue was purified by column chromatography through silica gel, eluting with *n*-hexane:ethyl acetate (7:3), to afford **5** (0.5075 g, 2.31 mmol, 89% yield) as a colorless oil. ^{1}H NMR (CDCl$_3$): δ 6.70 (d, J = 7.8 Hz, H5′), 6.65 (d, J = 1.8 Hz, H2′), 6.52 (dd, J = 7.8, 1.8 Hz, H6′), 5.92 (s, H10a, H10b), 4.25 (dd, J = 8.8, 7.2 Hz, H9′a), 3.96 (dd, J = 8.8, 6.4 Hz, H9′b), 2.74−2.82 (m, H8′), 2.61 (dd, J = 13.6, 8.3 Hz, H8a), 2.58 (dd, J = 13.6, 7.7 Hz, H8b), 2.50 (dd, J = 17.0, 7.7 Hz, H7′a), 2.23 (dd, J = 17.0, 6.8 Hz, H7′b). ^{1}H NMR (benzene-*d$_6$*): δ 6.66 (d, J = 7.8 Hz, H5′), 6.56 (d, J = 1.8 Hz, H2′), 6.52 (dd, J = 7.8, 1.8 Hz, H6′), 5.85 (s, H10a, H10b), 4.25 (dd, J = 9.1, 7.1 Hz, H9′a), 3.96 (dd, J = 9.1, 6.1 Hz, H9′b), 2.7 (ddtdd, J = 6.1, 6.8, 7.1, 8.1, 8.6 Hz, H8′), 2.62 (dd, J = 13.6, 7.1 Hz, H8b), 2.58 (dd, J = 13.6, 8.6 Hz, H8a), 2.51 (dd, J = 17.4, 8.1 Hz, H7′a), 2.18 (dd, J = 17.4, 6.8 Hz, H7′b). ^{13}C NMR (CDCl$_3$): δ 176.7 (C9), 147.9 (C5′), 146.3 (C4′), 131.9 (*C2′*), 121.5 (C1′), 108.8 (C3′), 108.3 (C6′), 100.9 (C10), 72.4 (C9′), 38.5 (C8), 37.2 (C8′), 33.9 (C7′). IR (cm^{-1}): 815 (C−H, Ar), 1156, 1267 (C−O), 1520 (C=C, Ar), 1772 (C=O), 2985, 3015 (C−H).

3,4,3′,4′-Bis(methylenedioxy)lignano-9,9′-lactone (Hinokinin, HK) (7). A solution of *n*-butyllithium (1.5 M in *n*-hexane, 1.2 mL, 1.82 mmol) was added dropwise to a stirred solution of diisopropylamine (0.1831 g, 1.82 mmol) in THF (5 mL) under inert atmosphere at 0 °C. After 15 min of agitation, the mixture was cooled to −78 °C and a solution of compound **5** (0.2001 g, 0.91 mmol) in THF (1 mL) was added. Piperonal (**1**) (0.1365 g, 0.91 mmol) was added after 1 h of agitation. The reaction was monitored by TLC, and after 4 h of agitation at −78 °C, the reaction mixture was warmed to 10 °C and quenched with a saturated solution of NH$_4$Cl. The resulting solution was extracted with ethyl acetate and the organic layer was dried over anhydrous magnesium sulfate. Evaporation of the solvent under reduced pressure gave a yellow oil that was purified by column chromatography through silica gel, eluting with *n*-hexane:ethyl acetate (4:6), to provide the epimeric alcohols **6** (0.3091 g, 0.77

Conformational Study of Lignanolactones

J. Phys. Chem. A, Vol. 111, No. 28, 2007 **6331**

mmol, 85% yield). ^{1}H NMR (CDCl$_3$): δ 7.0−6.2 (m, H Ar), 5.9 (s, 2H), 5.3 (d, J = 2.78 Hz, 1H), 4.85 (d, J = 8.3 Hz, 1H), 4.35 (dd, J = 7.8, 8.8 Hz, 1H), 4.1 (dd, J = 5.1, 8.3 Hz, 1H), 3.93 (dd, J = 5.6, 8.8 Hz, 1H), 3.86 (dd, J = 5.2, 8.8 Hz, 1H), 2.8 (m, 1H), 2.6 (m, 1H), 2.45 (m, 1H), 2.2 (m, 2H). Then, 5% palladium on activated carbon powder (0.2005 g) and a drop of 60% perchloric acid were added to a solution of epimers **6** (0.0701 g, 0.19 mmol) in methanol (10 mL). The resulting mixture was stirred under 4 atm of H$_2$ at room temperature for 60 h. The catalyst was removed by filtration through Celite and the solvent was evaporated under reduced pressure. The residue was purified by column chromatography through silica gel, eluting with *n*-hexane:ethyl acetate (8:2), to afford **7** (0.0537 g, 0.15 mmol, 80%). ^{1}H NMR (CDCl$_3$): δ 6.8−6.4 (m, H Ar), 5.9 (br s, 4H), 4.15 (dd, J = 7.1, 9.3 Hz, H9′a), 3.85 (dd, J = 7.1, 9.1 Hz, H9′b), 3.0 (dd, J = 5.1, 14.2 Hz, H7a), 2.85 (dd, J = 7.3, 14.2 Hz, H7b), 2.6 (dd, J = 7.1, 14.4 Hz, H7′a), 2.55 (m, H8), 2.45 (dd, J = 8.6, 14.4 Hz, H7′b), 2.4 (m, H8′). ^{13}C NMR (CDCl$_3$): δ 178.4 (C9), 147.9 (C3), 147.8 (C3′), 146.5 (C4), 146.4 (C4′), 131.6 (C1), 131.3 (C1′), 122.2 (*C2*), 121.55 (*C2′*), 109.4 (C5), 108.8 (C5′), 108.4 (C6), 108.3 (C6′), 101.0 (C10, C10′), 71.2 (C9′), 46.4 (C8), 41.3 (C8′), 38.4 (C7), 34.8 (C7′).

Supporting Information Available: Schemes showing CSD data mining and related structural studies, figures showing the Vista histograms, the three crystal structures for MDBL, and a structural comparison and tables of basis set convergence details and crystal packing effects evaluations, and text discussing the structural descriptors. This material is available free of charge via the Internet at http://pubs.acs.org.

References and Notes

(1) McRae, W. D.; Towers, G. H. N. Biological Activities of Lignans. *Phytochemistry* **1984**, *23*, 1207−1220.

(2) Ayres, D. C.; Loike, J. D. *Chemistry and Pharmacology of Natural Products: Lignans; Chemical, Biological and Clinical Properties*; Cambridge University Press: New York, 1990.

(3) Ward, R. S. Lignans, Neolignans, and Related Compounds. *Nat. Prod. Rep.* **1993**, *10*, 1−28.

(4) Ward, R. S. Lignans, Neolignans, and Related Compounds. *Nat. Prod. Rep.* **1995**, *12*, 183−205.

(5) Ward, R. S. Lignans, Neolignans, and Related Compounds. *Nat. Prod. Rep.* **1997**, *14*, 43−74.

(6) Ward, R. S. Lignans, Neolignans, and Related Compounds. *Nat. Prod. Rep.* **1999**, *16*, 75−96.

(7) Mann, J.; Davidson, R. S.; Hobbs, J. B.; Banthorpe, D. V.; Harborne, J. B. *Natural Products: Their Chemistry and Biological Significance*; Longman: Essex, U.K., 1994.

(8) Bastos, J. K.; Albuquerque, S.; Silva, M. L. A. Evaluation of the trypanocidal activity of lignans isolated from the leaves of *Zanthoxylum naranjillo. Planta Med.* **1999**, *65*, 541−544.

(9) Moss, G. P. Nomenclature of Lignans and Neolignans (IUPAC Recommendations 2000). *Pure Appl. Chem.* **2000**, *72*, 1493−1523.

(10) Bruno, I. J.; Cole, J. C.; Kessler, M.; Luo, J.; Motherwell, W. D. S.; Purkis, L. H.; Smith, B. R.; Taylor, R. Retrieval of Crystallographically-Derived Molecular Geometry Information. *J. Chem. Inf. Comput. Sci.* **2004**, *44*, 2133−2144.

(11) Allen, F. H.; Harris, S. E.; Taylor, R. Comparison of conformer distributions in the crystalline state with conformational energies calculated by ab initio techniques. *J. Comput.-Aided Mol. Des.* **1996**, *10*, 247−254.

(12) Boehm, H.-J.; Klebe, G. What can we learn from molecular recognition in protein-ligand complexes for the design of new drugs? *Angew. Chem., Int. Ed. Engl.* **1996**, *35*, 2588−2614.

(13) Bürgi, H. B. Structure Correlation and Chemistry. *Acta Crystallogr. A* **1998**, *54*, 873−885.

(14) Allen, F. H. The Development, Status and Scientific Impact of Crystallographical Databases. *Acta Crystallogr. A* **1998**, *54*, 758−771.

(15) Raithby, P. R.; Shields, G. P.; Allen, F. H. Conformational Analysis of Macrocyclic Ether Ligands. II. 1,4,7,10,13-Pentaoxacyclopentadecane and 1,4,7,10,13-Pentathiacyclopentadecane. *Acta Crystallogr. B* **1997**, *53*, 476−489.

(16) Munro, O. Q.; Mariah, L. Conformational analysis: Crystallographic, molecular mechanics and quantum chemical studies of C−H··· ·O hydrogen bonding in flexible bis(nosylate) derivatives of catechol. *Acta Crystallogr. B* **2004**, *60*, 598−608.

(17) Balacco, G. A Desktop Calculator for the Karplus Equation. *J. Chem. Inf. Comput. Sci.* **1996**, *36*, 885−887.

(18) Larue, L.; Gharbi-Benarous, J.; Archer, F.; Azerad, R.; Girault, J.-P. Conformational study in water by NMR and Molecular Modeling of Cyclic Glutamic Acid Analogues as Probes of Vitamin K Dependent Carboxylase. *J. Chem. Inf. Comput. Sci.* **1996**, *36*, 717−725.

(19) Grdadolnik, S. G.; Trebše, P.; Kočevar, M.; Solmajer, T. Structural Investigation of 5-Hydrazxono-5,6,7,8-tetrahydro-2*H*-1-benzopyran-2-ones and 5,6,7,8-Tetrahydroquinoline-2,5(1*H*)-diones. *J. Chem. Inf. Comput. Sci.* **1997**, *37*, 489−494.

(20) Navarro-Vázquez, A.; Cobas, J. C.; Sardina, F. C. A Graphical Tool for the Prediction of Vicinal Proton−Proton $^3J_{HH}$ Coupling Constants. *J. Chem. Inf. Comput. Sci.* **2004**, *44*, 1680−1685.

(21) Allen, F. H. The Cambridge Structural Database: a quarter of a million crystal structures and rising. *Acta Crystallogr. B* **2002**, *58*, 380−388.

(22) Fey, N.; Harris, S. E.; Harvey, J. N.; Orpen, A. G. Adding Value to Crystallographically-Derived Knowledge Bases. *J. Chem. Inf. Comput. Sci.* **2006**, *46*, 912−929.

(23) Kiralj, R.; Ferreira, M. M. C. Predicting Bond Lengths in Planar Benzenoid Polycyclic Aromatic Hydrocarbons: A Chemometric Approach. *J. Chem. Inf. Comput. Sci.* **2002**, *42*, 508−523.

(24) Kiralj, R.; Ferrreira, M. M. C. On Heteroaromaticity of Nucleobases. Bond Lengths as Multidimensional Phenomena. *J. Chem. Inf. Comput. Sci.* **2003**, *43*, 787−809.

(25) Krygowski, T. M. Crystallographic Studies of Inter- and Intramolecular Interactions Reflected in Aromatic Character of π-Electron Systems. *J. Chem. Inf. Comput. Sci.* **1993**, *33*, 70−78.

(26) Harris, P. E.; Orpen, A. G.; Bruno, I. J.; Taylor, R. Factors Affecting *d*-Block Metal-Ligand Bond Lengths: Toward an Automated Library of Molecular Geometry for Metal Complexes. *J. Chem. Inf. Mod.* **2005**, *45*, 1727−1748.

(27) Kämper, A.; Apostolakis, J.; Rarey, M.; Marian, C. M.; Lengauer, T. Fully Automated Flexible Docking of Ligands into Flexible Synthetic Receptor Using Forward and Inverse Docking Strategies. *J. Chem. Inf. Mod.* **2006**, *46*, 903−911.

(28) Klebe, G.; Mietzner, T. A fast and efficient method to generate biologically relevant conformations. *J. Comput.-Aided Mol. Des.* **1994**, *8*, 583−606.

(29) Feuston, M. P.; Miller, M. D.; Culberson, J. C.; Nachbar, R. B.; Kearsley, S. K. Comparison of Knowledge-Based and Distance Geometry Approaches for Generation of Molecular Conformations. *J. Chem. Inf. Comput. Sci.* **2001**, *41*, 754−763.

(30) Jones, G.; Willett, P.; Glen, R. C.; Leach, A. R.; Taylor, R. Development of validation of a genetic algorithm for flexible docking. *J. Mol. Biol.* **1997**, *267*, 727−748.

(31) Rarey, M.; Kramer, B.; Lengauer, T.; Klebe, G. A fast flexible docking method using an incremental construction algorithm. *J. Mol. Biol.* **1996**, *261*, 470−489.

(32) Lemmen, C.; Lengauer, T. Time-efficient flexible superposition of medium-sized molecules. *J. Comput.-Aided Mol. Des.* **1997**, *11*, 357−368.

(33) Stewart, J. J. P. Optimization of Parameters for Semiempirical Methods. 1. Methods. *J. Comput. Chem.* **1989**, *10*, 209−220.

(34) Ziegler, T. Approximate Density Functional Theory as a Practical Tool In Molecular Energetics and Dynamics. *Chem. Rev.* **1991**, *91*, 651−667.

(35) Becke, A. D. Density-Functional Thermochemistry. 3. The Role of Exact Exchange. *J. Chem. Phys.* **1993**, *98*, 5648−5652.

(36) Lee, C. T.; Yang, W. T.; Parr, R. G. Development of the Colle-Salvetti Correlation-Energy Formula Into A Functional Of The Electron Density. *Phys. Rev. B* **1988**, *37*, 785−789.

(37) *Titan 1.0.8*; Wavefunction, Inc.: Irvine, CA, 2001.

(38) *WebLab ViewerPro 4.0*; Accelrys, Inc.: Burlington, MA, 2000.

(39) *Chem3D Ultra 6.0*; CambridgeSoft.Com: Cambridge, MA, 2000.

(40) *Pirouette 3.01*; Infometrix, Inc.: Woodinville, WA, 2001.

(41) Matlab version 6.5.0.196271 Release 13.01. Mathworks, Inc.: Natick, MA, 2003.

(42) January 2006 Update of the *Cambridge Structural Database 5.27*; Cambridge Structural Data Centre, University of Cambridge: Cambridge, U.K., November 2005.

(43) Bruno, I. J.; Cole, J. C.; Edgington, P. R.; Kessler, M.; Macrae, C. F.; McCabe, P.; Pearson, J.; Taylor, R. New software for searching the Cambridge Structural Database and visualizing crystal structures. *Acta Crystallogr. B* **2002**, *58*, 389−397.

6332 *J. Phys. Chem. A, Vol. 111, No. 28, 2007*

Kiralj et al.

(44) ConQuest 1.8; Cambridge Structural Data Centre, University of Cambridge: Cambridge, U.K., 2005.

(45) Mercury 1.4.1; Cambridge Structural Data Centre, University of Cambridge: Cambridge, U.K., 2005.

(46) Vista 2.1c; Cambridge Structural Data Centre, University of Cambridge: Cambridge, U.K., 2005.

(47) Spek, T. PLATON−A Multipurpose Crystallographic Tool. *Acta Crystallogr. A* **1990**, *46*, C34.

(48) Farrugia, L. J. Platon for Windows. University of Glasgow 2005.

(49) Martens, H.; Naes, T. *Multivariate Calibration*, 2nd ed.; Wiley: New York, NY, 1989.

(50) Beebe, K. R.; Pell, R.; Sheasholtz, M. B. *Chemometrics: a practical guide*; Wiley: New York, 1998.

(51) Ferreira, M. M. C. Multivariate QSAR. *J. Braz. Chem. Soc.* **2002**, *13*, 742−753.

(52) Drew, M. G. B.; Harrison, R. J.; Mann, J.; Tench, A. J.; Young, R. J. Photoinduced addition of methanol to 5(*S*)-5-triisopropylsiloxymethyl-N-boc-dihydropyrrole-2(5*H*)-one: A new route to 4(*S*), 5(*S*)-disubstituted pyrrolidin-2-ones. *Tetrahedron* **1999**, *55*, 1163−1172.

(53) Kuehne, M. E.; Bornmann, W. G.; Parsons, W. H.; Spitzer, T. D.; Blount, J. F.; Zubieta, J. Total syntheses of (±)-cephalotaxine and (±)-8-oxocephalotaxine. *J. Org. Chem.* **1988**, *53*, 3439−3450.

(54) Syu, W., Jr.; Don, M.-J.; Lee, G.-H.; Sun, C.-M. Cytotoxic and Novel Compounds from *Solanum indicum*. *J. Nat. Prod.* **2001**, *64*, 1232−1233.

(55) Cremer, D.; Pople, J. A. General definition of ring puckering coordinates. *J. Am. Chem. Soc.* **1975**, *97*, 1354−1358.

(56) Kiralj, R.; Ferreira, M. M. C. Combined Computational and Chemometric Study of 1*H*-Indole-3-Acetic Acid. *Int. J. Quantum Chem.* **2003**, *95*, 237−251.

(57) Silva, M. C.; Kiralj, R.; Ferreira, M. M. C. Estudo Teórico da Interação Existente Entre a Artemisinina e Heme. *Quim. Nova* **2007**, *30*, 25−31.

(58) Stenutz, R. *Program for Calculation of Vicinal proton-proton coupling constants*; http://www.spectroscopynow.com/FCKeditor/UserFiles/File/specNOW/HTML%20files/proton-proton2.htm [last accessed on 21 March, 2007].

(59) Haasnoot, C. A. G.; DeLeeuw, F. A. A. M.; Altona, C. The relationship between proton-proton NMR coupling constants and substituent electronegativities. 1. An empirical generalization of the Karplus equation. *Tetrahedron* **1980**, *36*, 2783−2792.

(60) Altona, C. Vicinal Coupling Constants & Conformation of Bio-molecules. In *Encyclopedia of Nuclear Magnetic Resonance*; Grant, D. M., Harris, R. H., Eds.; J. Wiley & Sons Ltd.: Chichester, U.K., 1996; Vol. 8, pp 4909−4925.

(61) Landais, Y.; Robin, J. P.; Lebrun, A. Ruthenium dioxide in fluoro acid medium. 1. A new agent in the biaryl oxidative coupling. Application to the synthesis of non phenolic bisbenzocyclooctadiene lignan lactones. *Tetrahedron* **1991**, *47*, 3787−3804.

(62) Lopez, J. C.; Alonso, J. L.; Cervellati, R.; Esposti, A. D.; Lister, D. G.; Palmieri, P. Conformational and Ring Inversion in γ-Butyrolactone. Part 1−Microwave Spectrum. *J. Chem. Soc. Faraday Trans.* **1990**, *86*, 453−458.

(63) Esposti, D. D.; Alonso, J. L.; Cervellati, R.; Lister, D. G.; Lopez, J. C.; Palmieri, P. Conformational and Ring Inversion in γ-Butyrolactone. Part 2−Ab initio and Flexible Model Computations. *J. Chem. Soc. Faraday Trans.* **1990**, *86*, 459−466.

(64) Masia, M.; Rey, R. Computational Study of γ-Butyrolactone and Li$^+$/γ-butyrolactone in Gas and Liquid Phases. *J. Phys. Chem. B* **2004**, *108*, 17992−18002.

(65) Charro, M. E.; Alonso, J. L. Barriers to Internal Rotation in β-Methyl-γ-Butyrolactone, 3-Methylcyclopentanone, and γ-Valerolactone from Fourier Transform Microwave Spectroscopy. *J. Mol. Spectrosc.* **1996**, *176*, 251−257.

(66) Lopez, J. C.; Alonso, J. L.; Pelaez, F. J. The Microwave Spectrum of α-Methyl-γ-butyrolactone. *J. Mol. Spectrosc.* **1988**, *131*, 9−20.

(67) Aakeröy, C. B.; Seddon, K. R. The Hydrogen Bond and Crystal Engineering. *Chem. Soc. Rev.* **1993**, *22*, 397−404.

(68) Hatu, T.; Sato, S.; Tamura, C. (*E*)-4-(2-hydroxyiminocyclopentyl-methyl)-phenylacetic acid. *Acta Crystallogr. C* **1986**, *42*, 452−454.

(69) Caminati, W.; Damiani, D.; Corbelli, G.; Velino, B.; Bock, C. W. Microwave-spectrum and ab initio calculations of ethylbenzene. Potential energy surface of the ethyl group torsion. *Mol. Phys.* **1991**, *74*, 885−895.

(70) Emsley, J. W.; DeLuca, G.; Celebre, G.; Longeri, M. The conformation of the aromatic rings reliative to the alkyl chain in 4-*n*-pentyl-4′-cyanobiphenyl. *Liquid Cryst.* **1996**, *20*, 569−575.

(71) Cinacchi, G.; Prampolini, G. DFT Study of the Torsional Potential in Ethylbenzene and Ethyxybenzene: The Smallest Prototypes of Alkyl- and Alkoxy-Aryl Mesogens. *J. Phys. Chem. A* **2003**, *107*, 5228−5232.

(72) Maté, B.; Suenram, R. D.; Lugez, C. Microwave studies of three alkylbenzenes: Ethyl, *n*-propyl, and *n*-butylbenzenes. *J. Chem. Phys.* **2000**, *113*, 192−199.

(73) Tong, X.; Ford, M. S.; Dessent, C. E. H.; Müller-Dethlefs, K. The effect of conformation on the ionization energetics of *n*-butylbenzene. I. A threshold ionization study. *J. Chem. Phys.* **2003**, *119*, 12908−12913.

(74) Ford, M. S.; Tong, X.; Dessent, C. E. H.; Müller-Dethlefs, K. The effect of conformation on the ionization energetics of *n*-butylbenzene. I. A zero electron kinetic energy photoelectron spectroscopy study with partial rotational resolution. *J. Chem. Phys.* **2003**, *119*, 12914−12920.

(75) Campanelli, A. R.; Ramondo, F.; Domenicano, A.; Hargittai, I. Molecular Structure and Conformation of *tert*-Butylbezenes: A Concerted Study by Gas-Phase Electron Diffraction and Theoretical Calculations. *J. Phys. Chem.* **1994**, *98*, 11046−11052.

(76) Anastasakos, L.; Wildman, T. A. The effect of internal rotation on the methyl CH-stretching overtone spectra of toluene and the xylenes. *J. Chem. Phys.* **1993**, *99*, 9453−9459.

(77) Chelli, R.; Gervasio, F. L.; Procacci, P.; Schettino, V. Stacking and T-shape Competition in Aromatic-Aromatic Amino Acid Interactions. *J. Am. Chem. Soc.* **2002**, *124*, 6133−6143.

(78) McGaughey, G. B.; Gagnés, M.; Rappé, A. K. π-Stacking Interactions. *J. Biol. Chem.* **1998**, *273*, 15458−15463.

(79) Aravinda, S.; Shamala, N.; Das, C.; Srivanjini, A.; Karle, I. L.; Balaram, P. Aromatic-Aromatic Interactions in Crystal Structures of Helical Peptide Scaffolds Containing Projecting Phenylalanine Residues. *J. Am. Chem. Soc.* **2003**, *125*, 5308−5315.

(80) Sony, S. M. M.; Ponnuswamy, M. N. Nature of π-interactions in nitrogen-containing heterocyclic systems: A structural database analysis. *Cryst. Growth Des.* **2006**, *6*, 736−742.

(81) Honda, T.; Kimura, N.; Sato, S.; Kato, D.; Tominaga, H. Chiral Synthesis of Lignan Lactones, (−)-Hinokinin, (−)-Deoxypodorhizone, (−)-Isobalactone and (−)-Savinin by Means of Enantioselective Deprotonation. *J. Chem. Soc., Perkin Trans.* **1994**, *1*, 1043−1046.

(82) Bode, J. W.; Doyle, M. P.; Protopopova, M. N.; Zhou, Q.-L. Intramolecular Regioselective Insertion into Unactivated Prochiral Carbon−Hydrogen Bonds with Diazoacetates of Primary Alcohols Catalyzed by Chiral Dirhodium(II) Carboxamidates. Highly Enantioselective Total Synthesis of Natural Lignan Lactones. *J. Org. Chem.* **1996**, *61*, 9146−9155.

(83) Sakakibara, N.; Suzuki, S.; Umezawa, T.; Shimada, M. Biosynthesis of yatein in *Anthriscus sylvestris*. *Org. Biomol. Chem.* **2003**, *1*, 2474−2484.

(84) Takekawa, Y.; Shishido, K. Fragmentation Reactions of Optically Active Trisubstituted Cyclopropylcarbinyl Radicals. *J. Org. Chem.* **2001**, *66*, 8490−8503.

(85) Itoh, T.; Chika, J.-I.; Takagi, Y.; Nishiyama, S. An Efficient Enantioselective Total Synthesis of Antitumor Lignans: Synthesis of Enantiomerically Pure 4-Hydroxyalkanenitriles *via* an Enzymatic Reaction. *J. Org. Chem.* **1993**, *58*, 5717−5723.

(86) Brinksma, J.; van der Deen, H.; van Oeveren, A.; Feringa, B. L. Enantioselective synthesis of benzylbutyrolactones from 5-hydroxyfuran-2(5*H*)-one. New chiral synthons for dibenzylbutyrolactone lignans by a chemoenzymatic route. *J. Chem. Soc., Perkin Trans.* **1998**, *1*, 4159−4163.

(87) Vanderlei, J. M. L.; Coelho, F.; Almeida, W. P. A Simple and Stereoselective Synthesis of (+)-β-Piperonyl-γ-butyrolactone. *Synth. Commun.* **1998**, *28*, 3047−3055.

(88) Srikrishna, A.; Danieldoss, S. Radical Cyclisation Based Approach to Lignans. Synthesis of 4-Arylmethyldihydrofuran-2-ones. *Synth. Commun.* **2001**, *31*, 2357−2364.

(89) Morimoto, T.; Nagai, H.; Achiwa, K. Lipase-Catalyzed Esterification of a (±)-2,3-Di(arylmethyl)-1,4-butanediol and Its Application to the Synthesis of (*S*,*S*)-(+)-Hinokinin. *Synth. Commun.* **2005**, *35*, 857−865.

(90) Souza, V. A.; Silva, R.; Pereira, A. C.; Royo, V. A.; Saraiva, J.; Montanheiro, M.; Souza, G. H. B.; Silva, A. A. F.; Grando, M. D.; Donate, P. M.; Bastos, J. K.; Albuquerque, S.; Silva, M. L. A. Trypanocidal activity of (−)-cubebin derivatives against free amastigote forms of *Trypanosoma cruzi*. *Bioorg. Med. Chem. Lett.* **2005**, *15*, 303−307.

(91) Rehnberg, N.; Magnusson, G. General conjugate-addition method for the synthesis of enantiomerically pure lignans. Total synthesis of (−)- and (+)-burseran, (−)-dehydroxycubebin, (−)-trichostin, (−)-cubebin, (−)-5″-methoxyhinokinin, and (−)-hinokinin. *J. Org. Chem.* **1990**, *55*, 4340−4349.

(92) Belletire, J. L.; Fry, D. F. Oxidative Coupling of Carboxylic Acid Dianions: The Total Synthesis of (±)-Hinokinin and (±)-Fomentaric Acid. *J. Org. Chem.* **1987**, *52*, 2549−2555.

(93) Heleno, V. C. G.; Silva, R.; Pedersoli, S.; Albuquerque, S.; Bastos, J. K.; Silva, M. L. A.; Donate, P. M.; Silva, G. V. J.; Lopes, J. L. C. Detailed ^{1}H and ^{13}C NMR structural assignment of three biologically active lignan lactones. *Spectrochim. Acta A* **2005**, *63*, 234−239.

(94) Vaz, E.; Fernández, I.; Muñoz, L.; Llor, J. Conformational Equilibria of 7-Benzyl-2-iodo-9-oxa-7-azabicyclo[4.3.0]nonan-8-one in Solution. Correlations between Conformational Distribution and Solvent Solvatochromic Parameters. *J. Org. Chem.* **2006**, *71*, 2558−2564.

(95) Tvaroška, I.; Taravel, F. R.; Utille, J. P.; Carver, J. P. Quantum mechanical and NMR spectroscopy studies on the conformations of the hydroxymethyl and methoxymethyl groups in aldohexosides. *Carbohydr. Res.* **2002**, *337*, 353−367.

Conformational Study of Lignanolactones

J. Phys. Chem. A, Vol. 111, No. 28, 2007 **6333**

(96) Höfinger, S.; Zerbetto, F. The Free Energy of Nanobubbles in Organic Liquids. *J. Phys. Chem. A* **2003**, *107*, 11253−11257.

(97) Gonçalves, P. F. B.; Stassen, H. Free Energy of Solvation from Molecular Dynamics Simulations for Low Dielectric Solvents. *J. Comput. Chem.* **2003**, *24*, 1758−1765.

(98) Hippler, M. Quantum-chemical study of $CHCl_3$−SO_2 association. *J. Chem. Phys.* **2005**, *123*, 204311.1−204311.11.

(99) Chung, S.; Hippler, M. Infrared spectroscopy of hydrogen-bonded $CHCl_3$−SO_2 in the gas phase. *J. Chem. Phys.* **2006**, *124*, 214316.1−214316.7.

(100) Ribeiro-Claro, P. J. A.; Vaz, P. D. Towards the understanding of the spectroscopic behaviour of the C−H oscillator in C−H···O hydrogen bonds: the effect of solvent polarity. *Chem. Phys. Lett.* **2004**, *390*, 358−361.

(101) Zheng, J.; Liu, Q.; Zhang, H.; Fang, D. Solvent effect on infrared spectra of methyl methacrylate in CCl_4/C_6H_{14}, $CHCl_3$/C_6H_{14} and C_2H_5OH/C_6H_{14} binary solvent systems. *Spectrochim. Acta A* **2004**, *60*, 3119−3123.

(102) Henn, M.; Jurkschat, K.; Mansfeld, D.; Mehring, M.; Schürmann, M. Synthesis and structure of and DFT-studies on 1,3,5-$[P(O)(i\text{-}PrO)_2]_3C_6H_3$ and its $CHCl_3$ adducts: analysis of the Cl_3C−H···OP hydrogen bond. *J. Mol. Struct.* **2004**, *697*, 213−220.

(103) Villa, A.; Mark, A. E. Calculation of the Free Energy of Solvation for Neutral Analogs of Amino Acid Side Chains. *J. Comput. Chem.* **2002**, *23*, 548−553.

(104) Chambers, C. C.; Hawkins, G. D.; Cramer, C. J.; Truhlar, D. G. Model for Aqueous Solvation Based on Class IV Atomic Charges and First Solvation Shell Effects. *J. Phys. Chem.* **1996**, *100*, 16385−16398.